

Published in final edited form as:

Nat Chem Biol. 2020 March 01; 16(3): 240–249. doi:10.1038/s41589-019-0453-9.

Biased M1-muscarinic-receptor-mutant mice inform the design of next-generation drugs

Sophie J. Bradley^{1,✉}, Colin Molloy¹, Paulina Valuskova¹, Louis Dwomoh¹, Miriam Scarpa¹, Mario Rossi¹, Lisa Finlayson¹, Kjell A. Svensson², Eyassu Chernet², Vanessa N. Barth², Karolina Gherbi^{3,4}, David A. Sykes^{3,5}, Caroline A. Wilson⁶, Rajendra Mistry⁷, Patrick M. Sexton⁸, Arthur Christopoulos⁸, Adrian J. Mogg², Elizabeth M. Rosethorne^{3,5}, Shuzo Sakata⁶, R. A. John Challiss⁷, Lisa M. Broad⁹, Andrew B. Tobin^{1,✉}

¹The Centre for Translational Pharmacology, Institute of Molecular, Cell and Systems Biology, College of Medical, Veterinary and Life Sciences, <https://ror.org/00vtgdb53> University of Glasgow, Glasgow, UK.

²Eli Lilly & Co, Neuroscience Discovery, Lilly Corporate Center, Indianapolis, IN, USA

³School of Life Sciences, Queen's Medical Centre, <https://ror.org/01ee9ar58> University of Nottingham, Nottingham, UK.

⁴Excellerate Bioscience Ltd, BioCity, Nottingham, UK

⁵Centre of Membrane and Protein and Receptors (COMPARE), <https://ror.org/03angcq70> University of Birmingham and <https://ror.org/01ee9ar58> University of Nottingham, Midlands, UK.

⁶Strathclyde Institute of Pharmacy and Biomedical Sciences, <https://ror.org/00n3w3b69> University of Strathclyde, Glasgow, UK.

⁷Department of Molecular and Cell Biology, Henry Wellcome Building, <https://ror.org/04h699437> University of Leicester, Leicester, UK.

⁸Drug Discovery Biology, Monash Institute of Pharmaceutical Sciences and Department of Pharmacology, <https://ror.org/02bfwt286> Monash University, Parkville, Victoria, Australia.

⁹Eli Lilly & Co, Neuroscience Discovery, Erl Wood Manor, Windlesham, Surrey, UK

[✉] Correspondence and requests for materials should be addressed to S.J.B. or A.B.T. sophie.bradley@glasgow.ac.uk; andrew.tobin@glasgow.ac.uk.

Publisher's note Springer Nature remains neutral with regard to jurisdictional claims in published maps and institutional affiliations.

Author contributions

S.J.B. and A.B.T. devised the program of work and wrote the paper with assistance from all other authors. S.J.B., A.B.T., R.A.J.C., L.M.B., E.M.R., S.S., P.M.S., A.J.M. and A.C. designed and advised on experiments. L.D. conducted receptor phosphorylation studies. C.M. and L.F. managed the mouse colony and conducted mouse behavioral experiments with S.J.B. P.V., C.A.W. and L.F. conducted the EEG recording studies. M.S., M.R. and R.M. conducted signaling and internalization studies. K.A.S., E.C. and V.N.B. conducted in vivo receptor occupancy and in vivo ligand activity assays. K.G. and D.A.S. conducted arrestin assays.

Competing interests

The authors declare no competing interests.

Additional information

Supplementary information is available for this paper at <https://doi.org/10.1038/s41589-019-0453-9>.

Reprints and permissions information is available at www.nature.com/reprints.

Abstract

Cholinesterase inhibitors, the current frontline symptomatic treatment for Alzheimer's disease (AD), are associated with low efficacy and adverse effects. M1 muscarinic acetylcholine receptors (M1 mAChRs) represent a potential alternate therapeutic target; however, drug discovery programs focused on this G protein-coupled receptor (GPCR) have failed, largely due to cholinergic adverse responses. Employing novel chemogenetic and phosphorylation-deficient, G protein-biased, mouse models, paired with a toolbox of probe molecules, we establish previously unappreciated pharmacologically targetable M1 mAChR neurological processes, including anxiety-like behaviors and hyper-locomotion. By mapping the upstream signaling pathways regulating these responses, we determine the importance of receptor phosphorylation-dependent signaling in driving clinically relevant outcomes and in controlling adverse effects including 'epileptic-like' seizures. We conclude that M1 mAChR ligands that promote receptor phosphorylation-dependent signaling would protect against cholinergic adverse effects in addition to driving beneficial responses such as learning and memory and anxiolytic behavior relevant for the treatment of AD.

Alzheimer's disease (AD) is the most common form of dementia, affecting ~850,000 people in the UK and 50 million worldwide. Like many forms of dementia, AD is associated with a spectrum of symptoms that includes memory loss, but also behavioral disturbances such as anxiety and agitation. A single treatment strategy that might address the multiple components of AD has yet to emerge. The underlying basis of symptomatic treatment of AD is instead centered on addressing cognitive deficits by the restoration of cholinergic transmission via the inhibition of acetylcholinesterase, the enzyme responsible for the breakdown of acetylcholine¹. However, the efficacy of this treatment is limited by serious dose-related cholinergic adverse responses due primarily to the whole-body upregulation of cholinergic systems, both central and peripheral^{2,3}.

A widely considered alternate strategy has been to target the M1 muscarinic acetylcholine receptors (M1 mAChRs), one of five members (M1–M5) of a family of G protein-coupled receptors (GPCRs) that respond to acetylcholine and that show pro-cognitive effects in preclinical animal studies^{4–8}. However, despite some positive indications of efficacy in clinical trials, the M1/M4 preferring orthosteric agonist xanomeline⁹ and the bitopic agonist GSK1034702^{10–12} failed due to adverse cholinergic effects. An alternate strategy, designed to reduce adverse responses by increasing the selectivity for the M1 mAChR, is to target non-conserved allosteric sites that would positively modulate receptor activity, so-called positive allosteric modulators (PAMs)¹³. Despite the discovery of a variety of structurally distinct M1 mAChR-selective PAMs⁷, some of these molecules have similarly run into issues with adverse responses, including temporal lobe seizures^{7,14,15}. These studies highlight the serious lack of appreciation of the subtle pharmacological and structural properties of both M1-selective PAMs and orthosteric/bitopic ligands that underlie clinically efficacious responses versus adverse outcomes^{10,15,16}.

Furthermore, the potential of utilizing the concept of biased signaling¹⁷ to avert the muscarinic adverse responses that have thwarted drug discovery has similarly lacked thorough investigation¹⁸. To realize the full potential of M1 mAChR biased ligands, it will be necessary to dissect the *in vivo* signaling pathways that mediate clinically

relevant M1 mAChR neurological processes, and distinguish these from pathways leading to adverse responses¹⁷. We address this challenge here by generating a G protein-biased M1 mAChR by removing receptor phosphorylation sites and thereby uncouple the receptor from phosphorylation/arrestin-dependent signaling. By knock-in of this G protein-biased receptor (M1-PD) into the gene locus of the wild-type M1 mAChR, we were able to assign neurological and peripheral responses to either G protein-dependent or receptor phosphorylation/arrestin-dependent signaling.

We combined this approach with a unique application of Designer Receptor Exclusively Activated by Designer Drug (DREADD) technology, where the introduction of mutations in transmembrane domains 3 and 5 of the M1 mAChR generated a receptor mutant (M1-DREADD) that was unresponsive to the natural ligand acetylcholine, but rather was activated by the otherwise inert chemical ligand clozapine N-oxide (CNO)¹⁹. Whereas many other studies have used muscarinic DREADDs to investigate the role of G protein signaling in neuronal processes²⁰, here, by knockin of the M1-DREADD coding sequence into the M1 mAChR gene locus, we express the M1-DREADD in place of the wild-type M1 mAChR in a study designed to define the role and ‘druggability’ of the M1 mAChR. We predicted that the phenotype of this mutant mouse would mimic that of M1-receptor knockout (M1-KO) mice because the M1-DREADD receptor does not respond to acetylcholine. However, unlike M1-KO mice, deficits resulting from a loss of M1 mAChR activity would be corrected in the M1-DREADD mice by treatment with CNO. In this way we reasoned we could define physiological responses that might be targetable by pharmacological activation of the M1 mAChR. Using this approach together with the M1-PD mice and a mouse line expressing a phosphorylation-deficient version of the M1-DREADD (M1-DREADD PD) we describe here that pharmacological targeting of the M1 mAChR not only impacts on learning and memory but can also correct disturbances in anxiety-related behaviors and hyperactivity, suggesting that M1 mAChR ligands hold the promise of treatment of a broad spectrum of symptoms associated with AD. By mapping the bimodal signaling pathways underlying the neurological and adverse responses of the M1 mAChR, we further conclude that ligands biased towards M1 mAChR phosphorylation/arrestin-dependent signaling will have efficacy in clinically relevant responses, while minimizing adverse effects including ‘epileptic-like’ seizures.

Results

Generation of the M1-DREADD mice

Consistent with previous studies¹⁹, the human wild-type M1 mAChR expressed in Chinese hamster ovary (CHO) cells was potently activated by acetylcholine while showing a weak response to CNO, in an inositol phosphate accumulation assay (Supplementary Table 1). CHO cells expressing the M1-DREADD receptor showed a significant (5,000-fold) reduction in the potency of acetylcholine while responding to CNO with nM potency (Supplementary Table 1). Targeting the M1 mAChR gene locus with a construct that, following homologous recombination, replaced the coding sequence of the M1 mAChR with the coding sequence of the M1-DREADD (Fig. 1a and Supplementary Fig. 1a–c) resulted in mice that transcribed the M1-DREADD mRNA in the hippocampus and cortex at levels

that were not significantly different from that of the M1 mAChR in wild-type animals (which refers to animals that express a wild-type M1 mAChR tagged at the C terminus with an HA-epitope tag) (Fig. 1b). Furthermore, the M1-DREADD protein was expressed at comparable levels to that of the wild-type receptor in the cortex of control mice, but slightly higher levels in the hippocampus (Fig. 1c,d and Supplementary Fig. 2). The M1-DREADD mice showed normal levels of breeding and indicators of good health.

To establish the sensitivity of the M1-DREADD expressed in the engineered mice to muscarinic ligands, coupling of the M1-DREADD to heterotrimeric G proteins was assessed in membranes prepared from the cortex. In these experiments, CNO showed no significant activity in cortical membranes prepared from wild-type animals, while the muscarinic agonist carbachol produced a robust increase in [³⁵S]GTPγS binding (Fig. 1e and Supplementary Table 2). In contrast, CNO produced a potent increase in G_{q/11} coupling in cortical membranes prepared from M1-DREADD mice, whereas carbachol failed to stimulate a response (Fig. 1f and Supplementary Table 2).

The M1-DREADD in our engineered mice was thus expressed near equivalently to that of the M1 mAChR in wild-type mice and was not activated by the natural ligand acetylcholine, but was instead activated by CNO.

CNO reduces hyper-anxiety levels in M1-DREADD mice

M1-KO animals showed an increased anxiety-like phenotype in an elevated plus maze (EPM) test, as demonstrated by significantly fewer entries into the open arms of the maze compared to controls (Fig. 2a–g). M1-DREADD mice similarly showed fewer entries into the open arms of the maze (relative to total entries) compared to controls, indicating that the M1-DREADD animals mimicked the phenotype of the M1-KO mice (Fig. 2a–g). The hyper-anxiety phenotype shown by the M1-DREADD mice was restored to normal levels by the administration of CNO (0.3 mg kg⁻¹) 30 min before the behavioral test (Fig. 2a–g). Previous pharmacokinetic studies from our laboratory determined that 0.3 mg kg⁻¹ CNO administration (intraperitoneally, i.p.) gave a plasma exposure of ~50 nM (ref. ²¹), a concentration sufficient to fully activate virally expressed muscarinic DREADDs in vivo. Importantly, CNO (0.3 mg kg⁻¹, i.p.) had no effects on the wild-type mice nor the M1-KO mice in the EPM (Fig. 2a–g). These data indicate that loss of M1-AChR function results in an anxiety-like phenotype that is restored by direct activation of M1 mAChRs through selective ligands.

Hyperactivity of M1-DREADD mice is restored by CNO

Consistent with previous studies²², we confirm that M1-KO mice are hyperactive in an open field test (Fig. 2h–k; see Fig. 4e,g–k later). Because M1-DREADD is not responsive to the natural ligand, acetylcholine, mice expressing the M1-DREADD similarly displayed a hyper-locomotion phenotype (Fig. 2h–k). The hyper-locomotion associated with both M1-KO and M1-DREADD animals was also evident when the mice were tested in a Y maze paradigm (Fig. 2l and Supplementary Fig. 3). Importantly, administration of CNO (0.3 mg kg⁻¹) had no significant effects on the locomotion of wild-type or M1-KO mice, but reduced the hyper-locomotion observed in M1-DREADD animals to levels similar to that seen in

vehicle-treated control animals (Fig. 2g,l and Supplementary Fig. 3). These data indicate that not only are M1 mAChRs involved in regulating locomotion, but that modulation of locomotion is ‘druggable’ via selective agonism of this receptor subtype.

Generation of a phosphorylation-deficient M1 mAChR mouse

Like many other GPCRs, muscarinic receptors operate through two signaling arms—via heterotrimeric G proteins and receptor phosphorylation regulated pathways²³. The latter includes receptor coupling to arrestin-adaptor proteins and activation of arrestin-dependent processes such as receptor internalization²⁴. A mutant M1 mAChR that lacked all of the MS-identified phosphorylation sites²⁵ and other potential sites in the third intracellular loop and C-terminal tail (20 serine–alanine substitutions in total; Fig. 3a) was generated and expressed in HEK293 cells. This mutant receptor showed robust coupling to G_{q/11}/calcium mobilization (Fig. 3b and Supplementary Table 3) while showing reduced agonist-mediated receptor recruitment of arrestin (Fig. 3c and Supplementary Table 3) and a deficit in receptor internalization (Fig. 3d and Supplementary Fig. 4). These results are consistent with the notion that the phosphorylation-deficient receptor is ‘G protein-biased’.

A receptor knock-in mouse that expressed the phosphorylation-deficient form of the mouse M1 mAChR was generated (termed M1-PD; Supplementary Fig. 5). By comparing this mouse line with wild-type controls (that express a C-terminally tagged wild-type M1 mAChR) and M1-KO animals, it was our aim to differentiate between physiological responses that lie downstream of receptor phosphorylation-dependent signaling and those mediated by G protein activation. Radioligand binding assays determined that muscarinic-receptor expression in M1-PD mice in the cortex was equivalent to that in wild-type mice (Fig. 3e). Transcription of the mutant receptor in the cortex and hippocampus of M1-PD mice was not significantly different from that of the M1 mAChR in control animals (Fig. 3f) and quantification of western blotting results revealed no significant difference in the expression levels of the mutant M1 mAChR in the hippocampus and cortex of M1-PD mice (Fig. 3g,h and Supplementary Fig. 6). Finally, the coupling to heterotrimeric G proteins (as determined in [³⁵S]GTPγS assays and inositol 1,4,5-trisphosphate mass assays) of the M1 mAChR and phosphorylation-deficient variant was equivalent in cortical tissue extracts (Fig. 3i,j and Supplementary Table 3).

Neurophysiology regulated by M1 mAChR phosphorylation

We first tested the anxiolytic response in the M1-PD mice and found that, similar to the M1-KO mice, the M1-PD mice showed fewer entries into the open arms of an EPM (Fig. 4a–e). This indicates that anxiolytic responses revealed in the studies above are mediated by receptor phosphorylation-dependent signaling. Similarly, in a Y maze spontaneous alternation paradigm testing spatial working memory, the M1-PD mice showed significant deficit, indicating that, like the M1 mAChR-mediated anxiolytic response, this behavior is also under the positive regulation of receptor phosphorylation (Fig. 4f).

Locomotion was initially assessed in the open field test where M1-PD mice did not mimic the hyperactivity phenotype of M1-KO mice (Fig. 4g–j). Instead, in this test (Fig. 4j) and in the EPM (Fig. 4e), the total distance traveled by the M1-PD mice was less than the

wild-type, indicating that these mice were hypoactive. Interestingly, although locomotion monitored over a 24 h period using telemetry showed the M1-KO mice to be hyperactive, consistent with the above data, under this paradigm the M1-PD showed activity equivalent to wild-type mice (Fig. 4k). The conclusion from these locomotion studies was that, in contrast to the anxiolytic and spatial working memory responses, regulation of locomotor behavior is not dependent on receptor phosphorylation, but appears to be regulated in a G protein-dependent manner. The hypo-locomotion response observed in some of the tests (EPM and Y maze) might indicate that, although mediated by G protein pathways, M1 mAChR locomotion might be desensitized by receptor phosphorylation, resulting in hypo-locomotion when phosphorylation sites are removed (Fig. 4e,j).

We next compared these central responses with M1 mAChR-mediated salivary secretion. M1-KO mice showed reduced salivary secretion in response to the muscarinic-receptor agonist pilocarpine, as previously described²⁶, but this was not mimicked by the M1-PD mice (Fig. 4l) indicating that this response is also downstream of G protein-dependent signaling (summarized in Fig. 4m).

M1 mAChR phosphorylation reduces adverse responses

To further probe the role of receptor phosphorylation-dependent signaling in M1 mAChR-mediated responses, an M1-DREADD receptor was generated where the phosphorylation sites had been removed (Fig. 5a). In *in vitro* inositol phosphate assays, this phosphorylation-deficient DREADD receptor was activated by CNO with similar potency and efficacy to the fully phosphorylatable version of M1-DREADD (Supplementary Fig. 7a and Supplementary Table 1). Consistent with a role for receptor phosphorylation in driving phosphorylation/arrestin-dependent processes, the phosphorylation-deficient M1-DREADD was defective in agonist (CNO)-mediated receptor internalization (Supplementary Fig. 7b,c).

A knock-in mouse expressing the phosphorylation-deficient M1-DREADD in place of the M1 mAChR was generated and termed M1-DREADD PD (Supplementary Fig. 8a,b). The M1-DREADD PD mutant was transcribed at levels equivalent to that of the M1-DREADD receptor in M1-DREADD mice and the M1 mAChR in wild-type mice (Fig. 5b).

Possibly due to the fact that the M1-DREADD receptor is not activated by endogenous acetylcholine, the levels of expression of this receptor in hippocampus (but not the cortex) of engineered mice were slightly higher than that of the wild-type receptor (Supplementary Fig. 2). The expression of M1-DREADD PD was also significantly higher than the wild-type receptor (Fig. 5c,d and Supplementary Fig. 2). Importantly, there were no statistically significant differences between the expression levels of M1-DREADD and M1-DREADD PD receptors in the hippocampus or cortex (Supplementary Fig. 2). This is relevant, because the M1-DREADD acts as the control for the M1-DREADD PD (we do not use wild-type mice as controls when looking at the phenotype of the M1-DREADD PD).

G protein coupling assays in cortical membranes derived from M1-DREADD and M1-DREADD PD showed that CNO stimulated robust increases in $G_{q/11}$ coupling in both variants whereas carbachol gave no significant increases (Fig. 5e,f and Supplementary Table

2). When normalized to expression levels we estimated that M1-DREADD PD signaling to G_q was ~1.5-fold higher than M1-DREADD.

CNO induces adverse responses in M1-DREADD PD mice

The aim here was to investigate if physiological responses mediated by CNO administration to animals expressing the M1-DREADD receptor were similarly responsive in M1-DREADD PD mice. In this way we might further predict the impact of biased M1 mAChR-selective ligands. However, administration of CNO to M1-DREADD PD mice resulted in profound adverse responses (Supplementary Table 4), including both central and peripheral responses such as gastrointestinal disturbances and salivary hyper-secretion. These adverse responses have previously been associated with the failure of muscarinic drug discovery programs^{9,12,14,27–30}. Most striking, however, were the severe seizures characteristic of cholinergic temporal lobe ‘epileptic-like’ seizures^{31–33}. We further characterized these seizures using surface EEG recordings to monitor cortical activity (Fig. 5g,h). CNO induced a reduction in EEG power following CNO administration, followed by sporadic seizure activity, which subsequently developed into full epileptic-like episodes around 25–35 min after CNO administration. Importantly, the same dose of CNO (0.3 mg kg⁻¹) administered to M1-DREADD mice had no adverse effects (Supplementary Table 4).

G protein-biased systems show enhanced adverse responses

These data led to the prediction that a muscarinic-receptor ligand biased toward G protein-dependent signaling versus receptor phosphorylation-dependent signaling will show more adverse responses than a non-biased ligand. To test this prediction, we profiled the G protein/receptor phosphorylation bias of two well-characterized muscarinic ligands, pilocarpine³¹ and GSK1034702^{10–12}. Both these ligands stimulated $G_{q/11}$ -dependent signaling to inositol phosphate accumulation and activation of extracellular signal-regulated kinase 1/2 (pERK1/2) (Fig. 6a,b). Similarly, both pilocarpine and GSK1034702 stimulated phosphorylation of serine 228 in the third intracellular loop of the M1 mAChR, a site previously shown to be highly sensitive to agonist-mediated phosphorylation²⁵ (Supplementary Table 5 and Fig. 6c). Fitting the concentration–response curves to the operational model of agonism, we derived a transduction coefficient (τ) for each of the responses. By comparing these with the transduction coefficient of the natural ligand acetylcholine, we calculated the bias of the two ligands between G protein coupling and receptor phosphorylation, expressed as a bias factor (Supplementary Table 6 and Fig. 6d). This analysis determined that pilocarpine showed bias toward G protein signaling, whereas GSK1034702 showed no bias between G protein coupling and receptor phosphorylation pathways (Supplementary Table 6 and Fig. 6d).

That these ligands show similar properties *in vivo* was investigated by administration of either pilocarpine (30 mg kg⁻¹) or GSK1034702 (10 mg kg⁻¹) at doses that resulted in equivalent levels of receptor occupancy (60%) in rats, as determined using an M1 mAChR positron emission tomography (PET) tracer, LSN3172176³⁴ (Supplementary Fig. 9). At this dose, pilocarpine resulted in a robust inositol phosphate response that was approximately twofold greater than that observed for GSK1034702 (Fig. 6e,f), supporting the conclusion

that pilocarpine is more efficacious in stimulating G protein-dependent signaling compared to GSK1034702 in brain tissue.

We then examined adverse events in response to these two ligands in wild-type and M1-PD mice using doses that gave equivalent receptor occupancy. Consistent with the notion that ligands biased towards G protein signaling would show more pronounced adverse responses, we observed that pilocarpine induced significant central (tremors, grasping and convulsions) and peripheral (piloerection, lacrimation and diarrhea) adverse responses in both wild-type and M1-PD mice (Supplementary Table 7). Interestingly, salivation was the only response that was lower in the M1-PD than in WT mice in response to pilocarpine (Supplementary Table 7). Although this might point to salivation being downstream of receptor phosphorylation-dependent signaling, the data in Fig. 5I would point to this response being solely G protein-mediated. In contrast to pilocarpine, GSK1034702, which showed no stimulus bias, also showed no adverse responses in WT mice. It is only in the M1-PD mice (that is, in a mouse background where the receptor is G protein-biased) where adverse central and peripheral responses were observed with this ligand (Supplementary Table 8).

We next took advantage of an earlier finding from our laboratory that the bitopic nature of GSK1034702 binding to M1 mAChR meant that GSK1034702 acted as an agonist at both wild-type M1 mAChR and M1-DREADD receptors¹⁰. This means that this ligand could uniquely be used as an agonist in wild-type mice, as well as M1-DREADD and M1-DREADD PD mice. Administration of GSK1034702 at a dose that had no adverse effects in M1-DREADD mice (30 mg kg⁻¹) had profound peripheral and central adverse effects in M1-DREADD PD mice (Supplementary Table 9), a result consistent with the notion that M1 mAChR signal transduction that is biased toward G protein coupling results in adverse central and peripheral cholinergic responses.

Discussion

In this study we have generated a series of novel chemogenetic and G protein-biased mouse models that not only reveal the importance of phosphorylation/arrestin-dependent signaling in M1 mAChR-mediated learning and memory and anxiolytic behaviors, but also establish that the phosphorylation status of the M1 mAChR significantly contributes to minimizing cholinergic adverse effects. These adverse effects, both peripheral SLUDGE effects (salivation, lacrimation, urination, defecation, gastrointestinal disturbance and emesis) and central adverse responses, such as seizures, have represented one of the major barriers to the success of targeting muscarinic receptors in AD^{30,35}. Furthermore, our data suggest that, in addition to pro-cognitive benefits, targeting the M1 mAChR in AD might also have an impact on the associated behavioral abnormalities, including anxiety and hyperactivity.

By employing DREADD knock-in mice, we not only mimic the pharmacological activation of M1 mAChRs, but also reveal something of the nature of acetylcholine neurosignaling, as it would appear that cholinergic tone, disrupted in AD, can be mimicked by pharmacological agents, allowing for 'normal' neuronal activity and behavioral responses in a background where cholinergic transmission has been compromised.

In this study we wanted to determine the potential of employing the concept of biased ligands in directing M1 mAChR signaling to therapeutically beneficial pathways by mapping those responses that lie downstream of G protein-dependent versus phosphorylation/arrestin pathways (summarized in Fig. 4m). To do this, we generated a G protein-biased M1 mAChR by deleting all the potential phospho-acceptor sites. Interestingly, removal of these phosphorylation sites reduced, but did not eliminate, the interaction of the receptor with arrestin. This is in contrast to other GPCR subtypes where removal of phosphorylation sites results in almost complete absence of receptor/arrestin interaction³⁶. GPCRs can interact with arrestins via both a phosphorylation-dependent interaction with the phospho-sensor and via interaction with the activation sensor³⁷. Structural studies are revealing the molecular basis for this bimodal binding^{38,39}, in particular the role of the differential phosphorylation patterns driving different arrestin conformations and signaling outputs^{40,41}, supporting the hypothesis of a phosphorylation barcode^{42,43}. Here, we report that the interaction of the M1 mAChR with arrestin, similar to that previously reported for the M3 mAChR^{23,44,45}, is only partially dependent on the phosphorylation status of the receptor, indicating that the activation sensor on arrestin plays an equally important role as the phosphorylation sensor for the interaction of the M1 mAChR with arrestin. This may be significant when interpreting the phenotypic data of the M1-PD mice, because the phenotypes identified here as being dependent on the phosphorylation status of the M1 mAChR might not necessarily be due to a deficiency in receptor/arrestin interaction. Rather, it is possible that receptor phosphorylation is important for the correct assembly/activity of M1 mAChR signaling complexes in neurons in a manner that is independent of arrestin.

Classically, phosphorylation of GPCRs is related to receptor desensitization^{46,47}. Hence, one explanation for the phenotypes observed in the M1-PD mice might be that the receptor is unable to undergo phosphorylation-dependent desensitization. That this might be the case was illustrated by examination of the locomotion response. In agreement with previous studies^{22,48}, we demonstrate that M1-KO mice are hyperactive, indicating a role for the M1 mAChR in reducing locomotion. However, M1-PD mice are hypoactive, a result that might be interpreted to mean that the phosphorylation-deficient receptor itself is over-active, possibly due to a lack of desensitization.

However, when we assess the coupling of the phosphorylation-deficient receptor to G protein signaling in membranes and cortical slices from tissues derived from M1-PD mice, we see only a very small increase in coupling to G protein signaling. Furthermore, salivary secretion, which we show here is downstream of G protein coupling, is not significantly affected in M1-PD mice. These data point to the intriguing possibility that some physiological responses mediated by G protein signaling are desensitized by receptor phosphorylation (for example, locomotion), while others (for example, salivary secretion) are not.

The impact of biased signaling on cholinergic adverse responses was strikingly revealed in a set of experiments employing a G protein-biased M1-DREADD mutant mouse. In this mouse line we found that administration of CNO, at concentrations that caused no adverse responses in wild-type or M1-DREADD mice, resulted in profound peripheral and central

adverse responses, including seizures. Whereas it is clear from previous studies that adverse responses might be related to the degree of efficacy of muscarinic ligands (including the extent of cooperativity and intrinsic activity of PAMs)^{7,15}, there has not been any previous indication that receptor phosphorylation-dependent processes might have a role in regulating adverse responses. Given our data, it might be anticipated that ligands showing signaling bias away from receptor phosphorylation pathways and towards G protein coupling might show more pronounced cholinergic adverse responses. This was found to be the case with pilocarpine, which we show here to be both G protein-biased and possessing pronounced seizurogenic activity (consistent with previous studies^{31–33}). In contrast, GSK1034702, which was not biased, showed no seizures when administered to wild-type mice at a dose that gave the same receptor occupancy as pilocarpine. Interestingly, GSK1034702 only induced cholinergic adverse responses in phosphorylation-deficient, G protein-biased mice (that is, M1-PD and M1-DREADD PD). These data point to muscarinic ligands with a bias toward receptor phosphorylation-dependent signaling as having a lower propensity to mediating adverse responses.

Our study adds to a growing body of evidence that M1 mAChRs can be responsible for peripheral adverse effects previously thought to be mediated by M2/M3 receptors^{27,29,49}. Hence, simply developing highly selective M1 mAChR agonists might not be sufficient to avert cholinergic side effects. This conclusion is supported by reports that selective M1 mAChR PAMs also display adverse cholinergic responses^{7,14,15}. These adverse events appear to be linked with intrinsic activity, because those PAMs possessing high agonist activity also show cholinergic adverse responses^{7,14,15}, while those PAMs devoid of intrinsic agonist activity induce no cholinergic toxicity^{7,50}. What is not clear, and a point that certainly deserves further investigation, is whether PAMs that possess high agonist activity and significant adverse responses are also biased toward G protein signaling. That this may be the case is supported by data where those PAMs inducing adverse responses (for example, PF-06767832 and PF-06827443) also stimulate robust inositol phosphate signaling (indicative of G_q-signaling) in striatal tissue^{14,29}.

Given these studies, and taking into consideration our findings, we conclude that to minimize cholinergic side effects while delivering maximal clinical efficacy across a range of AD symptoms, next-generation M1 mAChR ligands should, in addition to being highly selective and have carefully calibrated efficacy, also drive receptor phosphorylation-dependent signaling.

online content

Any Nature Research reporting summaries, source data, extended data, supplementary information, acknowledgements, peer review information; details of author contributions and competing interests; and statements of data and code availability are available at <https://doi.org/10.1038/s41589-019-0453-9>.

Methods

Animal maintenance

All mice were bred as homozygous onto a C57BL/6J background. Male and female animals at 8–12 weeks old were used if not stated otherwise. Mice were fed ad libitum with a standard mouse chow and were maintained within the animal facility at least one week prior to experiments. Animals were cared for in accordance with national guidelines on animal experimentation. All experiments were performed under a project license from the British Home Office (UK) under the Animals (Scientific Procedures) Act of 1986.

Generation of M1-PD, M1-DREADD and M1-DREADD PD knock-in animals

For the generation of the knock-in animals, a construct containing the loxP-Stop-loxP cassette upstream of a sequence encoding for the M1-HA, M1-PD, M1-DREADD or M1-DREADD PD was generated and inserted within the encoding exon (exon 3) of the M1 mAChR gene (*Chmrl*). All constructs were tagged with a HA-epitope sequence (YPYDVDPDYA) appended to the C terminus. The M1-DREADD is the coding sequence for the humanized (humanizing mutations V5A, S254T, K320R, G337A and V413I) M1 mAChR, with two mutations Y106C and A196C (Fig. 1a). The M1-PD is the coding sequence of the mouse M1 mAChR, with mutations in the third intracellular loop and C-terminal tail that replace 20 serine residues with alanine (Fig. 4a). The M1-DREADD PD is the coding sequence for the humanized M1-DREADD plus 20 serine–alanine mutations in the third intracellular loop and C-terminal tail (Fig. 6a).

The targeting vectors containing the coding sequences for the muscarinic-receptor mutants were subsequently transfected into embryonic stem (ES) cells derived from C57BL/6J mice, and neomycin-resistant ES cells were selected. Homologous recombination was validated by PCR and Southern blot. Recombined ES cell clones were injected into blastocysts for the generation of chimeric mice. Breeding of chimeras with C57BL/6 and Cre-recombinase expressing mice allowed the generation of heterozygous mice. Heterozygous animals were bred for the generation of homozygous lines. M1-KO mice were conditional M1-PD mice expressing a Stop of transcription cassette flanked with loxP sites upstream of the M1-PD cDNA. To obtain these mice please contact the corresponding authors. The generation of M1-HA, M1-PD, M1-DREADD, M1-DREADD PD and M1-KO mice was carried out by genOway.

Note that the M1-KO strain was generated using conditional M1-PD mice that were not crossed with any CRE-deleter strains, therefore leaving the stop cassette upstream of the ATG intact and resulting in a mouse strain where the receptor was not expressed (see the summary of the construct in Supplementary Fig. 4).

Quantitative polymerase chain reaction with reverse transcription

RNA was isolated from hippocampus or cortex of WT, M1-DREADD, M1-DREADD PD, M1-PD or M1-KO mice using a Qiagen lipid tissue RNeasy kit according to the manufacturer's instructions. RNA concentration was quantified using a Nanodrop and 1 µg total RNA template per reaction was used for cDNA synthesis using SuperScript III

first-strand synthesis SuperMix (Invitrogen). RNA/water (total 8 μ l), 2 μ l RT enzyme and 10 μ l 2 \times RT reaction mix were mixed together and incubated for 10 min at 25 $^{\circ}$ C, followed by 30 min at 50 $^{\circ}$ C, then 5 min at 85 $^{\circ}$ C. Samples were then chilled on ice. Each reaction was performed in the presence and absence of RT enzyme (–RT control). Finally, cDNA was incubated with 1 μ l (2 U) of *E. coli* RNase H and at 37 $^{\circ}$ C for 20 min and subsequently stored at –20 $^{\circ}$ C until qRT–PCR was performed.

For qRT–PCR, the following M1 mAChR primers were used (at 300:300 dilution):

F: 5' CAAGTGGCATTTCATCGGGATCACC

R: 5' GAGAAAGTGCCAATGATGAGATCAGC

Each reaction was performed in triplicate. Each reaction was performed in a total volume of 25 μ l containing 12.5 μ l SYBR Green Master Mix, 0.75 μ l F primer (10 μ M stock), 0.75 μ l R primer (10 μ M stock), 10 μ l water and 1 μ l cDNA (or –RT sample).

IP1 accumulation assay—Human M1-WT or M1-DREADD PD constructs were stably expressed in CHO-Flp-In cells and grown to confluence in T75 cm^2 flasks in Ham's F12 medium containing 10% FBS and 1% penicillin/streptomycin and under hygromycin B selection (400 μ g ml^{-1}). Cells were harvested and centrifuged at 1,000 g for 3 min before resuspension in 1 \times stimulation buffer (HEPES, 10 mM; CaCl_2 , 1 mM; MgCl_2 , 0.5 mM; KCl, 4.2 mM; NaCl, 146 mM; glucose, 5.5 mM; LiCl, 50 mM; pH 7.4) at 1.43×10^6 cells ml^{-1} . Test compounds (7 μ l per well) and cell suspension (7 μ l per well) were added to 384-well white ProxiPlates (PerkinElmer). Following a brief centrifugation, plates were incubated at 37 $^{\circ}$ C for 45 min. The IP1-d2 conjugate and the anti-IP1 cryptate Tb conjugate (IP1 Tb assay kit, CisBio) were diluted 1:30 in lysis buffer and 3 μ l of each were added to each well. The plate was incubated at 37 $^{\circ}$ C for 1 h and fluorescence resonance energy transfer (FRET) between d2-conjugated IP1 (emission at 665 nm) and Lumi4-Tb cryptate conjugated anti-IP1 antibody (emission at 620 nm) was detected using an Envision plate reader (PerkinElmer). Results were calculated from the 665/620 nm ratio and normalized to the maximum response stimulated by ACh.

ERK1/2 phosphorylation—Stimulation of ERK1/2 phosphorylation (Thr 202/Tyr 204) was assessed using the CisBio Phospho-ERK Cellular Assay Kit. Confluent monolayers of CHO Flp-In cells stably expressing the human M1 mAChR were serum starved overnight before the experiment. Cells were washed with 100 μ l PBS and incubated in serum-free F12 medium at 37 $^{\circ}$ C. Cells were stimulated with test compounds for 5 min at 37 $^{\circ}$ C in a final volume of 200 μ l. The stimulations were terminated by rapid aspiration and addition of 50 μ l lysis buffer supplemented with blocking reagent. Lysates were gently agitated at room temperature for 30 min. Subsequently, 16 μ l of this lysate was transferred to a 384-well white ProxiPlate (PerkinElmer) and incubated with 4 μ l premixed antibody solution for 2 h at room temperature. Fluorescence emission (665 and 620 nm) was determined using a PHERAstar plate reader (BMG Labtech).

Cell culture and transfection (for Ca²⁺ and β -arrestin recruitment assays)—

PathHunter HEK293: β -arrestin:EA cells were transfected with the mouse WT or the mouse phosphorylation-deficient M1 mAChR in the ProLink vector (DiscoverX), and grown under antibiotic selection (G418) to produce a stable pool of cells expressing the receptor. HEK293 wt/pdM₁: β -arrestin:EA cells were maintained in DMEM medium containing l-glutamine supplemented with FBS (10% vol/vol), hygromycin B (250 μ g ml⁻¹) and geneticin G418 (500 μ g ml⁻¹) at 37 °C, 5% CO₂.

Intracellular Ca²⁺ measurement—PathHunter HEK293 wt/pdM₁: β -arrestin cells were seeded into 96-well clear-bottomed, black plates (Costar) at 40,000 cells per well in 90 μ l cell culture medium and incubated at 37 °C, 5% CO₂ overnight to achieve a confluent monolayer. On the day of the experiment, 30 μ l of 4 \times Ca²⁺ no-wash assay kit 4 (Molecular Devices) containing 0.02% pluronic acid:2.5 mM probenecid (1:1) was added to each well of the 96-well cell plate and incubated at 37 °C, 5% CO₂ for 30 min. Agonist-induced changes in intracellular calcium (Ca²⁺) concentration were then monitored over time using a FlexStation 3 (Molecular Devices). Basal fluorescence was monitored for 16 s before addition of a range of M1 mACh receptor agonists, after which changes in fluorescence were recorded for a further 60 s. Responses to agonist were expressed as change in fluorescence from baseline to peak. The maximum fluorescence was taken as the highest point of the initial peak following agonist addition. The minimum fluorescence was taken as the background fluorescence prior to agonist addition.

Arrestin recruitment assay—PathHunter HEK293 wt/pdM₁: β -arrestin cells were seeded overnight in white, clear-bottomed 384-well ViewPlates (PerkinElmer) at 8,000 cells per well in 20 μ l cell culture medium and incubated at 37 °C, 5% CO₂ overnight to achieve a confluent monolayer. On the day of the assay, spent medium was removed and replaced with HBSS containing 0.1% BSA (wt/vol) and 20 mM HEPES, at pH 7.4. Cells were stimulated with a range of M1 mACh receptor agonists for 2 h (in 5 μ l), after which 25 μ l or proprietary Flash detection reagent (DiscoverRx) was added and plate incubated for 15 min at room temperature in the dark. Luminescence was read on a ClarioStar system (BMG) using the Luminescent protocol with no filter.

Western blotting

Preparation of membrane extracts: Membrane extracts were prepared following a protocol similar to the membrane preparation described in refs. ^{4,51}. Briefly, hippocampi were homogenized by sonication at 3–5 μ g amplitude in 25 mM sodium phosphate buffer, pH 7.4, and containing proteinase inhibitors. Samples were then centrifuged at 20,000g for 30 min at 4 °C. The pellets were incubated with 1.2% digitonin in 25 mM sodium phosphate and 5 mM MgCl₂ buffer (pH 7.4) overnight at 4 °C, with end-over-end rotation. After centrifugation of samples at 20,000g for 30 min at 4 °C, the supernatants (membrane extracts) were transferred to fresh microcentrifuge tubes and stored at –80 °C until use. Protein concentrations were determined by using the Micro BCA protein assay reagent kit according to the manufacturer's instructions.

Western blotting analysis—Samples were incubated with Laemmli loading buffer containing 5% β -mercaptoethanol for 30 min at 37 °C and loaded in 7.5% SDS-Tris-glycine polyacrylamide gels. Samples were run at ± 100 V following transfer onto nitrocellulose membranes that were blocked for 2 h with 5% fat-free milk in TBS-T (0.1% Tween-20 in TBS at pH 7.4). Membranes were then incubated with the respective primary antibody overnight at 4 °C, then washed three times with TBS-T (10 min each wash) and incubated with the respective secondary antibody (1:5,000) conjugated to horseradish peroxidase. Proteins were visualized with the ECL detection system (Signal West Pico PLUS Chemiluminescent substrate #34578).

[³H]-NMS binding—Membrane preparations of mouse hippocampus or cortex (50 μ g per tube) were incubated in binding buffer (HEPES, 50 mM; NaCl, 110 mM; KCl, 5.4 mM; CaCl₂, 1.8 mM; MgSO₄, 1 mM; glucose, 25 mM; sucrose, 58 mM; pH 7.4) containing increasing concentrations (0.1–5 nM) of [³H]-NMS for 1 h at 37 °C. Membrane-bound ligand was separated from free ligand by rapid filtration onto GF/B glass microfiber filters followed by three washes with ice-cold 0.9% NaCl. Membrane-bound radioactivity was determined by liquid scintillation (PerkinElmer Ultima Gold) counting. Non-specific binding was determined in the presence of atropine (1 μ M) during the incubation with [³H]-NMS.

[³⁵S]-GTP γ S assay—M1-WT, M1-DREADD, M1-PD and M1-DREADD PD (8–12 weeks) were humanely killed, then cortical tissue was dissected on ice. Tissue was suspended in ice-cold buffer A (containing 0.9% (wt/vol) NaCl, 10 mM HEPES, 0.2% (wt/vol) EDTA, pH 7.4) and homogenized (4 \times 5 s bursts) using a Polytron homogenizer. The suspension was centrifuged at 200g for 5 min at 4 °C using an Eppendorf 5810R bench-top centrifuge. Supernatants were collected and rehomogenized as above. The suspension was subsequently centrifuged for 20 min at 40,000g at 4 °C using a Beckman Coulter Avanti JXN-26 centrifuge with a JA-25.25 rotor. The supernatant was discarded and the pellet was resuspended in 10 ml ice-cold buffer B (10 mM HEPES, 10 mM EDTA, pH 7.4). The pellet was homogenized, GTP (1 mM final) was added and the suspension was incubated at 37 °C for 15 min. The suspension was subsequently centrifuged for 20 min at 40,000g at 4 °C and the pellet was resuspended in 15 ml ice-cold buffer C (10 mM HEPES, 0.1 mM EDTA, pH 7.4) and rehomogenized as before. The suspension was centrifuged again for 20 min at 40,000g at 4 °C. The final pellet was resuspended in buffer C and the protein concentration was estimated using a Bradford assay. The homogenate was then further diluted in final storage buffer to produce a concentration of 2 mg ml⁻¹.

[³⁵S]-GTP γ S binding and immunoprecipitation of G α subunits was performed as previously described^{4,51}. Specifically, M1-WT, M1-DREADD, M1-PD or M1-DREADD PD membranes were diluted in assay buffer (HEPES, 10 mM; NaCl, 100 mM; MgCl₂, 10 mM; pH 7.4) containing a final concentration of 1 μ M GDP. Membranes (75 μ g in a total assay volume of 200 μ l) were added to [³⁵S]-GTP γ S (1 nM final concentration) and agonists (CCh or CNO) and incubated at 30 °C for 5 min. Reactions were terminated by the addition of 1 ml ice-cold assay buffer and immediate transfer to an ice bath. Samples were centrifuged (20,000g, 6 min, 4 °C) and membrane pellets solubilized by the addition

of 50 μ l ice-cold solubilization buffer (100 mM Tris HCl, 200 mM NaCl, 1 mM EDTA, 1.25% Igepal and 0.2% SDS, pH 7.4) and incubation for 1 h at 4 °C on a shaking platform. Following complete protein resolubilization, 50 μ l of solubilization buffer without SDS was added. Solubilized protein was precleared using normal rabbit serum at a dilution of 1:100 and 3% (wt/vol) protein A–sepharose beads in TE buffer (10 mM Tris HCl, 10 mM EDTA, pH 8.0) added for 60 min at 4 °C. Protein A–sepharose beads and insoluble material were collected by centrifugation (20,000g, 6 min, 4 °C) and 100 μ l of the supernatant was transferred to fresh tubes containing G_q-specific anti-serum (Santa Cruz, sc393) and incubated overnight at 4 °C. Protein A–sepharose beads were added to samples, vortex mixed and rotated at 4 °C for 90 min before being centrifuged (10,000g, 1 min, 4 °C). Supernatants were aspirated and the protein A–sepharose beads washed three times with ice-cold solubilization buffer (without SDS). Recovered beads were then mixed with 1 ml FloScint-IV scintillation cocktail and counted by liquid scintillation spectrometry.

Ins(1,4,5)P₃ mass assay—M1-HA or M1-PD mice were humanely killed via cervical dislocation. The brain was exposed and transferred to an ice-cold platter and the cerebral cortex was dissected. The cerebral cortex was cross-chopped using a McIlwain tissue chopper (300 μ m \times 300 μ m). The resulting tissue cubes were dispersed into Krebs–Henseleit buffer (KHB: NaCl, 118 mM; KCl, 4.7 mM; MgSO₄, 1.2 mM; NaHCO₃, 25 mM; NaH₂PO₄, 1.2 mM; CaCl₂, 1.3 mM; HEPES, 10 mM; glucose, 11 mM; pH 7.4 after equilibration with O₂/CO₂ 95:5), washed by multiple buffer changes and then shaken in an oscillating water bath for 60 min at 37 °C. Tissue cubes were sedimented under gravity and buffer was changed every 10 min during this period.

At the end of the washing period, cerebral cortex cubes were allowed to sediment under gravity, and 25 μ l aliquots of ‘packed’ tissue were transferred to a flat-bottomed 5 ml tube containing 250 μ l KHB. Each tube was purged with O₂/CO₂ (95:5), capped and returned to a shaking water bath at 37 °C. Drug additions were made (bringing the total incubation volume to 300 μ l), tubes were again purged with O₂/CO₂ (95:5) and incubations were continued for the times indicated in the figure legends. Incubations were terminated by addition of an equal volume of ice-cold 1 M trichloroacetic acid and tubes were allowed to extract on ice for 30 min. Tubes were then centrifuged (2,000g, 20 min, 4 °C). Supernatants were recovered, neutralized using the dichlorodifluoromethane/tri-*n*-octylamine method and inositol 1,4,5-trisphosphate (IP₃) concentration was determined exactly as described previously⁵². Tissue cube pellets were solubilized by addition of 1 M NaOH. Protein concentration was determined for each incubation using the Lowry method. This allowed IP₃ mass accumulation to be expressed as pmol IP₃ per mg protein.

Elevated plus maze—The mice were habituated to the EPM testing room overnight and were maintained in the dark until testing. Where mice received vehicle (5% glucose) or CNO (0.3 mg kg⁻¹), this was administered 30 min prior to the test via i.p. injection.

The EPM consisted of four non-transparent arms (50 \times 10 cm): two enclosed arms (with black walls of 30 cm height) and two dimly illuminated open arms. Mice were placed into the center of the elevated plus maze, facing the closed arm. Mice were tracked using ANY-maze software for 5 min, and the number of entries into the closed or open arms

during this time was monitored. Anxiety level was calculated as a percentage of open arm entries versus total entries made. The maze was cleaned with 70% ethanol between each animal.

Open field—General locomotor activity was assessed using the open field test, following overnight habituation in the behavioral testing suite. Mice were placed into a clear, Perspex square arena (50 × 50 cm) and activity was tracked for a 10 min period using ANY-maze software.

Y maze—Mice were habituated to the behavioral testing suite overnight before the test. For tests where mice received vehicle (5% glucose) or CNO (0.3 mg kg⁻¹), these were administered via i.p. injection 30 min before the start of the test. Mice were placed into the center of a Y maze (grey, non reflective base plate) with three identical arms (A, B and C; lane width, 5 cm; arm length, 35 cm; arm height, 10 cm). Activity was recorded using ANY-maze software. Spontaneous alternation behavior was calculated by measuring the number of ‘ABC’ sequences (in any order) as a proportion of the total triplet sequences made during the 8 min test.

In vivo telemetry—The basal locomotor activity was measured in intact freely moving wild-type, M1-PD and M1-KO mice using a telemetric system (Data Sciences International). TA-F10 implantable probes (1.1 ml; 1.6 g) were implanted in the peritoneal cavity under isoflurane (1.5–2%) anesthesia and carprofen (Rimadyl; 5 mg kg⁻¹ subcutaneously (s.c.)) analgesia. During implantation, the mice were kept on a thermostable pad. After surgery, mice were housed individually and left for recovery for one week before being used in the experiment. Basal locomotor activity was acquired directly from the transponders for three consecutive days, during which the animals were not disturbed. Locomotor activity was recorded in home cages. Receivers were connected through MX2 matrix directly to a PC into a single computer port, allowing for the determination of all parameters. The data were collected every 60 s and a Ponemah acquisition system (DSI) was used for collecting and first processing of the data.

Biorhythm analysis—The data from telemetry experiments collected by the Ponemah acquisition system (DSI) were grouped into 10 min sequences, and the calculated means were used for further analysis. The analysis was performed using the ChronosFit program⁵³ employing Fourier analysis and a stepwise regression technique.

Electroencephalogram recordings

Surgery and recording: Animals (M1-HA WT, M1-DREADD, M1-MDREADD PD) were anesthetized with isoflurane (1–1.5%) and placed in a stereotaxic frame (model SR-5M-HT, Narishige). Animal heads were shaved using electric clippers and cleaned with ethanol (70%) and iodopovidone. Lidocaine (2%, 0.1–0.3 mg) was administered s.c. at the site of incision and carprofen (Rimadyl; 5 mg kg⁻¹) was administered s.c. to provide analgesia after surgery. The body temperature of the animals was maintained at 37 °C using a heating pad during the entire surgery. Five bone screws were fixed in the skull, two in the frontal region (anterior to posterior (AP) + 1.5 mm, mid to lateral (ML) ± 1 mm from bregma) to be used

as electrodes for frontal cortical EEGs, two in the parietal region (AP – 2 mm, ML \pm 2 mm from bregma) to be used for parietal cortical EEGs and one on the cerebellum as a ground and a reference. The electrodes with screws were attached with dental cement as a head post. After the head post surgery, the animals were left to recover for at least five days before being used in the experiment. During the acclimation period of five days, the animals were handled on a daily basis, placed in the recording chamber and the animal's head tethered to the recording cable. The following day after the acclimation period, the animals were placed back in the recording chamber for electrophysiological recording.

The recording was performed as follows. The initial 15 min served for the recording of basal cortical activity. The mice were then injected (i.p.) with vehicle (5% glucose) or with CNO (0.3 mg kg⁻¹) and EEG recordings continued for another 45 min. During the entire experimental procedure, mice were allowed to move freely and were monitored for the occurrence of seizures.

After animals were anesthetized with isoflurane (1–1.5%), they were placed in a stereotaxic frame (SR-5M-HT, Narishige) then body temperature was maintained at 37 °C using a feedback temperature controller (50-7221-F, Harvard Bioscience). Lidocaine (2%, 0.1 ml) was administered s.c. at the site of incision and carprofen (Rimadyl, 5 mg kg⁻¹) was also administered s.c. at the back. After incision, the skull was exposed and cleaned. Four bone screws were implanted and used for cortical EEG recording. Another screw was implanted over the cerebellum as a ground and reference. All screws were connected with a connector and covered with dental cement. The animals were left to recover for at least five days.

Electrophysiological recording procedures are described elsewhere^{34,53}. Briefly, the animal was placed in an open box (21.5 cm \times 47 cm \times 20 cm) by connecting a 16-channel amplifier board (RHD2132, Intan Technologies) and an interface cable. Signals were amplified relative to a cerebellar bone screw and were digitized at 1,000 Hz (RHD2132 and RHD 2000, Intan Technologies). Each recording session consisted of a 15 min baseline recording, an i.p. injection (CNO 0.3 mg kg⁻¹ or vehicle) and another recording for at least 45 min.

All offline analysis was performed using MATLAB (version R2018b, Mathworks). Because all four EEG channels provided qualitatively similar signals, only the signals at the right frontal region were used. To compute a spectrogram, the multi-taper spectral estimation method was applied (Chronux Toolbox, <http://chronux.org/>). To evaluate signal power, a root-mean-square (r.m.s.) value was computed every 1 s and scaled in dB. After lowpass-filtering the scaled signals at 1/300 Hz, they were normalized relative to the baseline (the mean value of the first 5 min signals) to compare them across experiments.

Measurement of saliva secretion—Mice were anesthetized by i.p. injection with 100 mg kg⁻¹ of ketamine/0.25 mg kg⁻¹ of medetomidine. Following this procedure, mice were injected with pilocarpine (1 mg ml⁻¹, i.p.) and salivary secretion (in milligrams of saliva) onto GF/B filter paper (GE Healthcare Life Sciences) was recorded every 5 min over a 35 min period.

Immunocytochemistry for internalization of receptors—CHO cells stably expressing the HA-tagged (C-terminal) version of the mouse M1-WT, mouse M1-PD, humanized M1-DREADD or humanized M1-DREADD PD were grown for 24 h to achieve 60–80% confluence on 13 mm glass coverslips coated with 0.01% poly-d-lysine. Cells were stimulated with 100 μ M carbachol (WT and M1-PD) or CNO (M1-DREADD or M1-DREADD PD) for 1 h, fixed using 4% PFA (in TBS buffer), and blocked and permeabilized using 2% BSA in Triton X-100 (0.1% in TBS buffer). Incubation with anti-EEA1 polyclonal antibody (ThermoFisher Scientific; 1:1,000) was carried out at 4 °C overnight, and incubation with anti-HA antibody (Roche; 1:1,000) was performed at room temperature for 2 h. Following three washes with TBS buffer, secondary antibody incubation with AlexaFluor 594 anti-rabbit and AlexaFluor 488 anti-rabbit (ThermoFisher; 1:400) was performed for 2 h at room temperature, and followed by three quick washes with TBS. Coverslips with stained cells were mounted on glass slides using VECTASHIELD HardSet Antifade Mounting Medium with DAPI. Data were acquired using an LSM 880 confocal laser scanning microscope (Zeiss).

Rat inositol phosphate accumulation

Sample collection: Rat (Sprague–Dawley 250–275 g) brain samples (frontal cortex) were collected after animals were administered the following treatments: H₂O vehicle or LiCl (100 mg kg⁻¹, s.c.) followed 30 min later by H₂O vehicle or scopolamine (1 mg kg⁻¹, s.c.) or SKF38393 (20 mg kg⁻¹, s.c.) at a dose volume of 1 ml kg⁻¹. One hour post LiCl administration, rats were dosed with pilocarpine (10, 30 or 100 mg kg⁻¹, s.c.) or GSK1034702 (3, 10 or 30 mg kg⁻¹, i.p.). Rats were euthanized 2 h later and frontal cortex was collected over dry ice. Samples were stored at -70 °C for liquid chromatography (LC) with tandem mass spectrometry (MS/MS) analysis of inositol phosphate.

Mass spectrometry: Samples were homogenized using a probe sonicator set at level 8 for 10 s in 5× volumes of 50% acetonitrile containing 0.1% formic acid and 50% methanol (MeOH). Samples were then centrifuged for 12 min at 13,000g. A 100 μ l volume of supernatant was transferred into 200 μ l of distilled water and 20 μ l aliquots of samples were injected onto the LC/MS apparatus. Myo-inositol 2-monophosphate bis (cyclohexylammonium) salt (Sigma Aldrich, I5250) was used to prepare standards (10, 30, 100, 300 and 1,000 ng g⁻¹ or ml⁻¹) in 50% acetonitrile + 50% methanol + 0.1% formic acid). The analysis of inositol phosphate was carried out using an Agilent 6410 series triple quad LC–MS/MS with MassHunter data analysis software (Agilent Technologies) fitted with an electrospray ion source and run in negative mode. Detection was accomplished by monitoring the precursor ion of inositol phosphate with a mass to charge ratio (m/z) of 259 and targeting its product ion with m/z set to 78.9. The chromatographic separation employed a Zorbax RX-SIL HPLC column (2.1 × 150 mm, Agilent Technologies) and a mobile phase consisting of 3% acetonitrile in water with an overall 0.1% formic acid content with a flow rate of 0.7 ml min⁻¹. Clearly delineated chromatographic peaks with the retention time of authentic standards and expected molecular weight were seen after each injection of sample. Analyte were quantified based on the areas of these peaks.

In vivo receptor occupancy

Live phase: Male Sprague–Dawley rats ($n = 4$ per dose group) were purchased from Harlan (Indianapolis) and ranged in weight from 200 to 300 g. Pilocarpine or GSK1034702 was administered at doses of 0.03, 0.1, 0.3, 1, 3 and 10 mg kg⁻¹ for generation of a dose response. Animals received either vehicle alone (1% hydroxyethylcellulose, 0.25% polysorbate 80, 0.05% antifoam in purified water) or test compound in a dose volume of 10 ml kg⁻¹. In the dose–response studies, rats received i.v. administration of non-labeled tracer LSN3172176³⁴ 10 mg kg⁻¹, 0.5 ml kg⁻¹ dose volume for rats and 5 ml kg⁻¹ dose volume for mice, in the lateral tail vein 30 min after vehicle or compound administration. Animals were euthanized by cervical dislocation 20 min after tracer administration. Brains were removed and dissected. Frontal cortex and cerebellum were used for tracer measurement and the remaining brain and plasma were used for compound exposure analysis. The receptor occupancy was considered to be measured at the time of tracer administration, t . Studies were performed at Covance Alnwick or Greenfield.

Tissue preparation and tracer analysis: Frontal cortex and cerebellar samples were weighed and placed in conical centrifuge tubes on ice. Four volumes (wt/vol) of acetonitrile containing 0.1% formic acid was added to each tube. Samples were then homogenized using an ultrasonic probe and centrifuged using a bench-top centrifuge at 14,000 r.p.m. for 20 min. Supernatant was diluted by adding 50 μ l to 150 μ l sterile water in 96-well plates for LC–MS/MS analysis. Analysis of LSN3172176 was carried out using an API 4000 mass spectrometer.

Chromatographic separation employed an Agilent Zorbax Eclipse XDB-C18 column (2.1 \times 50 mm) and a gradient mobile phase consisting of 15–90% acetonitrile in water with an overall 0.1% formic acid content. Detection of LSN3172176 was accomplished by monitoring the precursor to product ion transition with a mass to charge ratio (m/z) of 386.3 to 128.0. Standards were prepared by adding known quantities of the tracer to brain tissue samples from non-treated rats or mice and processing as described above.

Receptor occupancy determinations: Receptor occupancy was calculated using the ratio method. The level of tracer was measured in each cortical and cerebellar sample. A ratio of cortical levels (total binding) to cerebellar levels (non-specific binding) was generated for each animal. Vehicle ratios represent 0% occupancy and a ratio of 1, where the binding in the cortex is equal to the binding in the cerebellum, represents 100% occupancy. The ratios from the pilocarpine and GSK1034702 pretreated groups were interpolated linearly between the ratio in the vehicle-treated animals (0% occupancy) and 1 (100% occupancy) in order to determine the percent M1 receptor occupancy. For the pilocarpine and GSK1034702 dose response, a curve was fitted to a four-parameter logistic function with the bottom and top fixed at 0% and 100%, respectively using GraphPad Prism version 6.0 and the dose achieving 50% receptor occupancy (RecOcc₅₀) was calculated by the software. Values are given as mean \pm s.e.m.

Data analysis—Functional concentration–response curves were fitted according to a four-parameter logistic equation (to determine minimum and maximum asymptotes, log half

maximal effective concentration (EC_{50}) and slope; GraphPad Prism 6). To assess agonist bias, the same concentration–response curves were analyzed according to a modified form of the operational model of agonism, recast to directly yield a transduction ratio ($\log(\tau/K_A)$; ref. ⁵⁴), where basal represents the response in the absence of agonist, E_m represents the maximal response of the assay system, K_A represents the equilibrium dissociation constant of the agonist, $[A]$ represents the concentration of agonist, τ is an index of the coupling efficiency (or efficacy) of the agonist, and n is the slope of the transducer function linking agonist occupancy to response. For the analysis, all families of agonist curves at each pathway were globally fitted to the model with the parameters, basal, E_m and n shared between all agonists. For full agonists, $\log K_A$ was constrained to a value of zero, whereas for partial agonists this was directly estimated by the curve fitting procedure; the $\log(\tau/K_A)$ parameter was estimated as a unique measure of activity for each agonist. Agonist bias factors ($-\log_{10}(\tau/K_A)$) were calculated as previously described⁵⁴.

Reporting Summary—Further information on research design is available in the Nature Research Reporting Summary linked to this article.

Supplementary Material

Refer to Web version on PubMed Central for supplementary material.

Acknowledgements

This work is funded by a University of Glasgow Lord Kelvin Adam Smith Fellowship (to S.J.B.), an MRC MICA agreement MR/P019366/1 (to A.B.T., S.J.B., M.R. and C.M.), a Wellcome Trust Collaborative Award 201529/Z/16/Z (to A.B.T., P.V., A.C., L.D., C.M. and P.M.S.), SULSA Dementia Seed Funding (to A.B.T., P.V. and S.S.), ARUK PPG2017B-005 (to S.S.) and an MRC iCASE studentship with Eli Lilly (M.S.). This work was also supported by an MRC group leader program awarded to A.B.T. at the MRC Toxicology Unit. We acknowledge support from the BSU facilities at the Cancer Research UK Beatson Institute (C596/A17196) and the Biological Services at the University of Glasgow. We also thank M. Gaellman for support to the Tobin laboratory.

Data availability

All data are available from the authors or are available through the University of Glasgow online data repository.

References

1. Bartus RT, Dean RL III, Beer B, Lippa AS. The cholinergic hypothesis of geriatric memory dysfunction. *Science*. 1982; 217: 408–414. [PubMed: 7046051]
2. Courtney C, et al. Long-term donepezil treatment in 565 patients with Alzheimer’s disease (AD2000): randomised double-blind trial. *Lancet*. 2004; 363: 2105–2115. [PubMed: 15220031]
3. Inglis F. The tolerability and safety of cholinesterase inhibitors in the treatment of dementia. *Int J Clin Pract*. 2002; 127: 45–63.
4. Bradley SJ, et al. M1 muscarinic allosteric modulators slow prion neurodegeneration and restore memory loss. *J Clin Invest*. 2017; 127: 487–499. [PubMed: 27991860]
5. Digby GJ, et al. Novel allosteric agonists of M1 muscarinic acetylcholine receptors induce brain region-specific responses that correspond with behavioral effects in animal models. *J Neurosci*. 2012; 32: 8532–8544. [PubMed: 22723693]

6. Ghoshal A, et al. Potentiation of M1 muscarinic receptor reverses plasticity deficits and negative and cognitive symptoms in a schizophrenia mouse model. *Neuropsychopharmacology*. 2016; 41: 598–610. [PubMed: 26108886]
7. Moran SP, et al. M₁-positive allosteric modulators lacking agonist activity provide the optimal profile for enhancing cognition. *Neuropsychopharmacology*. 2018; 43: 1763–1771. [PubMed: 29581537]
8. Shirey JK, et al. A selective allosteric potentiator of the M₁ muscarinic acetylcholine receptor increases activity of medial prefrontal cortical neurons and restores impairments in reversal learning. *J Neurosci*. 2009; 29: 14271–14286. [PubMed: 19906975]
9. Bodick NC, et al. Effects of xanomeline, a selective muscarinic receptor agonist, on cognitive function and behavioral symptoms in Alzheimer disease. *Arch Neurol*. 1997; 54: 465–473. [PubMed: 9109749]
10. Bradley SJ, et al. Bitopic binding mode of an M₁ muscarinic acetylcholine receptor agonist associated with adverse clinical trial outcomes. *Mol Pharmacol*. 2018; 93: 645–656. [PubMed: 29695609]
11. Budzik B, et al. Novel N-substituted benzimidazolones as potent, selective, CNS-penetrant, and orally active M₁ mAChR agonists. *ACS Med Chem Lett*. 2010; 1: 244–248. [PubMed: 24900202]
12. Nathan PJ, et al. The potent M1 receptor allosteric agonist GSK1034702 improves episodic memory in humans in the nicotine abstinence model of cognitive dysfunction. *Int J Neuropsychopharmacol*. 2013; 16: 721–731. [PubMed: 22932339]
13. Conn PJ, Christopoulos A, Lindsley CW. Allosteric modulators of GPCRs: a novel approach for the treatment of CNS disorders. *Nat Rev Drug Discov*. 2009; 8: 41–54. [PubMed: 19116626]
14. Davoren JE, et al. Design and synthesis of γ - and δ -lactam M₁ positive allosteric modulators (PAMs): convulsion and cholinergic toxicity of an M₁-selective PAM with weak agonist activity. *J Med Chem*. 2017; 60: 6649–6663. [PubMed: 28598634]
15. Rook JM, et al. Diverse effects on M1 signaling and adverse effect liability within a series of M₁ Ago-PAMs. *ACS Chem Neurosci*. 2017; 8: 866–883. [PubMed: 28001356]
16. Nickols HH, Conn PJ. Development of allosteric modulators of GPCRs for treatment of CNS disorders. *Neurobiol Dis*. 2014; 61: 55–71. [PubMed: 24076101]
17. Smith JS, Lefkowitz RJ, Rajagopal S. Biased signalling: from simple switches to allosteric microprocessors. *Nat Rev Drug Discov*. 2018; 17: 243–260. [PubMed: 29302067]
18. Marlo JE, et al. Discovery and characterization of novel allosteric potentiators of M₁ muscarinic receptors reveals multiple modes of activity. *Mol Pharmacol*. 2009; 75: 577–588. [PubMed: 19047481]
19. Armbruster BN, Li X, Pausch MH, Herlitze S, Roth BL. Evolving the lock to fit the key to create a family of G protein-coupled receptors potently activated by an inert ligand. *Proc Natl Acad Sci USA*. 2007; 104: 5163–5168. [PubMed: 17360345]
20. Roth BL. DREADDs for neuroscientists. *Neuron*. 2016; 89: 683–694. [PubMed: 26889809]
21. Thompson KJ, et al. DREADD agonist 21 is an effective agonist for muscarinic-based DREADDs in vitro and in vivo. *ACS Pharm Transl Sci*. 2018; 1: 61–72.
22. Gerber DJ, et al. Hyperactivity, elevated dopaminergic transmission, and response to amphetamine in M1 muscarinic acetylcholine receptor-deficient mice. *Proc Natl Acad Sci USA*. 2001; 98: 15312–15317. [PubMed: 11752469]
23. Bradley SJ, et al. Mapping physiological G protein-coupled receptor signaling pathways reveals a role for receptor phosphorylation in airway contraction. *Proc Natl Acad Sci USA*. 2016; 113: 4524–4529. [PubMed: 27071102]
24. Reiter E, Lefkowitz RJ. GRKs and β -arrestins: roles in receptor silencing, trafficking and signaling. *Trends Endocrinol Metab*. 2006; 17: 159–165. [PubMed: 16595179]
25. Butcher AJ, et al. An antibody biosensor establishes the activation of the M₁ muscarinic acetylcholine receptor during learning and memory. *J Biol Chem*. 2016; 291: 8862–8875. [PubMed: 26826123]
26. Gautam D, et al. Cholinergic stimulation of salivary secretion studied with M₁ and M₃ muscarinic receptor single- and double-knockout mice. *Mol Pharmacol*. 2004; 66: 260–267. [PubMed: 15266016]

27. Alt A, et al. Evidence for classical cholinergic toxicity associated with selective activation of M₁ muscarinic receptors. *J Pharmacol Exp Ther.* 2016; 356: 293–304. [PubMed: 26582730]
28. Bodick NC, et al. The selective muscarinic agonist xanomeline improves both the cognitive deficits and behavioral symptoms of Alzheimer disease. *Alzheimer Dis Assoc Disord.* 1997; 11: S16–S22. [PubMed: 9339268]
29. Davoren JE, et al. Discovery of the potent and selective M₁ PAM-agonist *N*-[(3*R*,4*S*)-3-hydroxytetrahydro-2*H*-pyran-4-yl]-5-methyl-4-[4-(1,3-thiazol-4-yl)benzyl]pyridine-2-carboxamide (PF-06767832): evaluation of efficacy and cholinergic side effects. *J Med Chem.* 2016; 59: 6313–6328. [PubMed: 27275946]
30. Felder CC, et al. Current status of muscarinic M₁ and M₄ receptors as drug targets for neurodegenerative diseases. *Neuropharmacology.* 2018; 136: 449–458. [PubMed: 29374561]
31. Cavalheiro EA, Santos NF, Priel MR. The pilocarpine model of epilepsy in mice. *Epilepsia.* 1996; 37: 1015–1019. [PubMed: 8822702]
32. Levesque M, Avoli M, Bernard C. Animal models of temporal lobe epilepsy following systemic chemoconvulsant administration. *J Neurosci Methods.* 2016; 260: 45–52. [PubMed: 25769270]
33. Turski WA, et al. Limbic seizures produced by pilocarpine in rats: behavioural, electroencephalographic and neuropathological study. *Behav Brain Res.* 1983; 9: 315–335. [PubMed: 6639740]
34. Mogg AJ, et al. In vitro pharmacological characterization and in vivo validation of LSN3172176 a novel M₁ selective muscarinic receptor agonist tracer molecule for positron emission tomography (PET). *J Pharmacol Exp Ther.* 2018; 365: 602–613. [PubMed: 29643252]
35. Bender AM, Jones CK, Lindsley CW. Classics in chemical neuroscience: xanomeline. *ACS Chem Neurosci.* 2017; 8: 435–443. [PubMed: 28141924]
36. Prihandoko R, et al. Distinct phosphorylation clusters determine the signaling outcome of free fatty acid receptor 4/G protein-coupled receptor 120. *Mol Pharmacol.* 2016; 89: 505–520. [PubMed: 26873857]
37. Gurevich VV, Gurevich EV. The structural basis of arrestin-mediated regulation of G-protein-coupled receptors. *Pharmacol Ther.* 2006; 110: 465–502. [PubMed: 16460808]
38. Shukla AK, et al. Structure of active β -arrestin-1 bound to a G-protein-coupled receptor phosphopeptide. *Nature.* 2013; 497: 137–141. [PubMed: 23604254]
39. Zhou XE, et al. Identification of phosphorylation codes for arrestin recruitment by G protein-coupled receptors. *Cell.* 2017; 170: 457–469. [PubMed: 28753425]
40. Mayer D, et al. Distinct G protein-coupled receptor phosphorylation motifs modulate arrestin affinity and activation and global conformation. *Nat Commun.* 2019; 10: 1261 [PubMed: 30890705]
41. Staus DP, et al. Sortase ligation enables homogeneous GPCR phosphorylation to reveal diversity in β -arrestin coupling. *Proc Natl Acad Sci USA.* 2018; 115: 3834–3839. [PubMed: 29581292]
42. Butcher AJ, et al. Differential G-protein-coupled receptor phosphorylation provides evidence for a signaling bar code. *J Biol Chem.* 2011; 286: 11506–11518. [PubMed: 21177246]
43. Nobles KN, et al. Distinct phosphorylation sites on the β_2 -adrenergic receptor establish a barcode that encodes differential functions of β -arrestin. *Sci Signal.* 2011; 4: ra51 [PubMed: 21868357]
44. Kong KC, et al. M₃-muscarinic receptor promotes insulin release via receptor phosphorylation/arrestin-dependent activation of protein kinase D1. *Proc Natl Acad Sci USA.* 2010; 107: 21181–21186. [PubMed: 21078968]
45. Poulin B, et al. The M₃-muscarinic receptor regulates learning and memory in a receptor phosphorylation/arrestin-dependent manner. *Proc Natl Acad Sci USA.* 2010; 107: 9440–9445. [PubMed: 20439723]
46. Lefkowitz RJ. A brief history of G-protein coupled receptors (Nobel Lecture). *Angew Chem.* 2013; 52: 6366–6378. [PubMed: 23650015]
47. Lefkowitz RJ. Historical review: a brief history and personal retrospective of seven-transmembrane receptors. *Trends Pharmacol Sci.* 2004; 25: 413–422. [PubMed: 15276710]
48. Miyakawa T, Yamada M, Duttaroy A, Wess J. Hyperactivity and intact hippocampus-dependent learning in mice lacking the M₁ muscarinic acetylcholine receptor. *J Neurosci.* 2001; 21: 5239–5250. [PubMed: 11438599]

49. Kurimoto E, et al. An approach to discovering novel muscarinic M₁ receptor positive allosteric modulators with potent cognitive improvement and minimized gastrointestinal dysfunction. *J Pharmacol Exp Ther.* 2018; 364: 28–37. [PubMed: 29025977]
50. Rook JM, et al. A novel M₁ PAM VU0486846 exerts efficacy in cognition models without displaying agonist activity or cholinergic toxicity. *ACS Chem Neurosci.* 2018; 9: 2274–2285. [PubMed: 29701957]

References

51. Challiss RA, Batty IH, Nahorski SR. Mass measurements of inositol(1,4,5)trisphosphate in rat cerebral cortex slices using a radioreceptor assay: effects of neurotransmitters and depolarization. *Biochem Biophys Res Commun.* 1988; 157: 684–691. [PubMed: 2904813]
52. Arraj M, Lemmer B. Circadian rhythms in heart rate, motility, and body temperature of wild-type C57 and eNOS knock-out mice under light-dark, free-run, and after time zone transition. *Chronobiol Int.* 2006; 23: 795–812. [PubMed: 16887749]
53. Lyngholm D, Sakata S. Cre-dependent optogenetic transgenic mice without early age-related hearing loss. *Front Aging Neurosci.* 2019; 11: 29. [PubMed: 30863301]
54. van der Westhuizen ET, Breton B, Christopoulos A, Bouvier M. Quantification of ligand bias for clinically relevant β_2 -adrenergic receptor ligands: implications for drug taxonomy. *Mol Pharmacol.* 2014; 85: 492–509. [PubMed: 24366668]

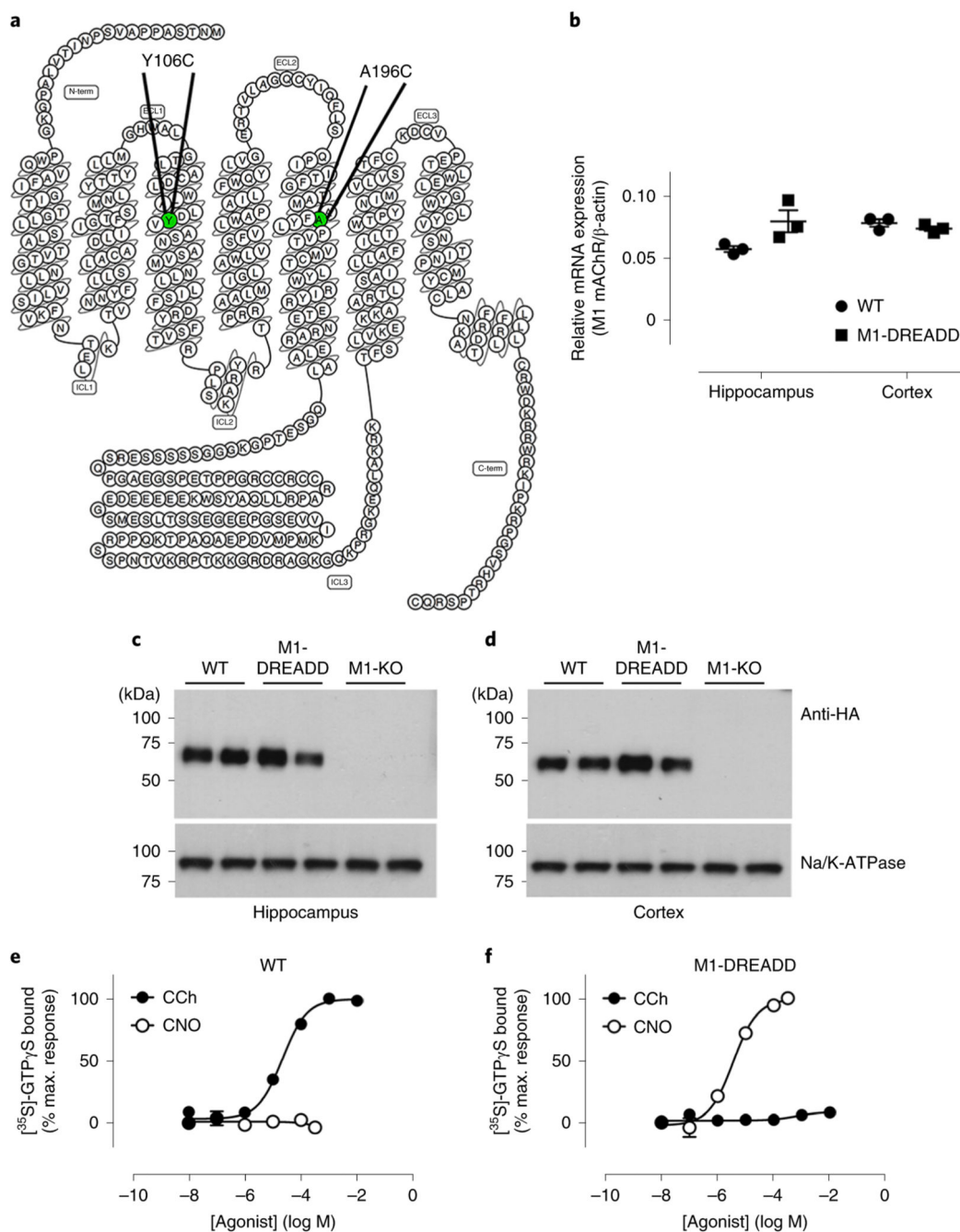


Fig. 1. Generation of the M1-DREADD knock-in mouse.

a, Snake plot of the M1 receptor identifying the mutations introduced to generate the M1-DREADD receptor. **b**, Quantitative polymerase chain reaction with reverse transcription (qRT-PCR) showing the transcription of M1 mAChR RNA in the hippocampus or cortex of wild-type (WT) or M1-DREADD mice. Data are expressed as a ratio of β -actin RNA transcription ($n = 3$ mice). **c,d**, Solubilized membranes prepared from the hippocampus (**c**) or cortex (**d**) of WT M1-HA, M1-DREADD and M1-KO mice were probed in a western blot analysis for the expression of M1 mAChR using an antibody for the HA tag. Data shown are

for two separate mice for each genotype. Similar data were obtained on at least two further occasions (Supplementary Fig. 2). Na^+/K^+ ATPase expression was used as a loading control. **e,f**, Stimulation of [^{35}S]-GTP γ S binding to cortical membranes prepared from WT (**e**) or M1-DREADD (**f**) mice following stimulation with carbachol (CCh) or clozapine N-oxide (CNO). Data are expressed as mean \pm s.e.m. of three to four independent experiments performed in duplicate and normalized to the maximal response at the WT receptor.

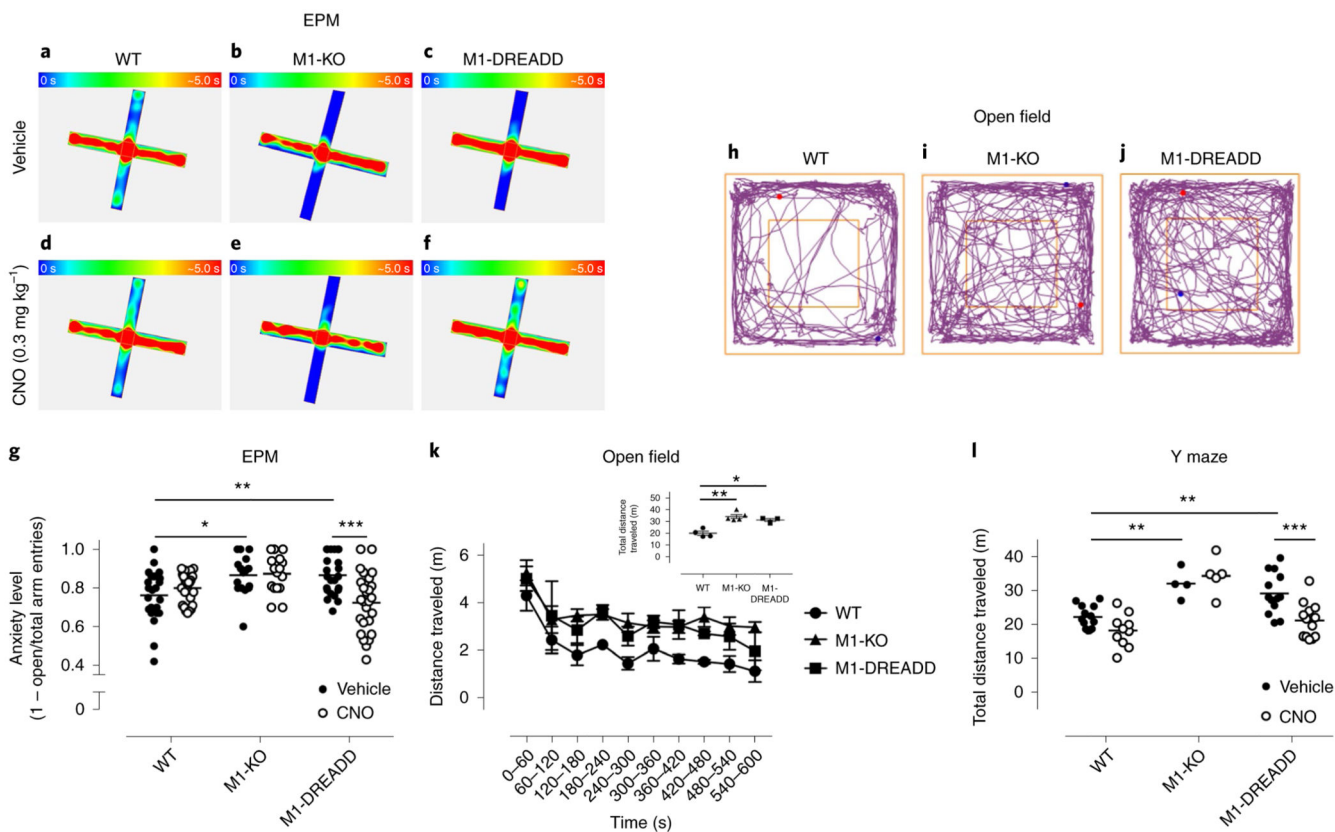


Fig. 2. Altered phenotypes of M1-DREADD mice are corrected by CNO.

a–f, Heat maps showing the occupancy of WT (**a,d**), M1-KO (**b,e**) and M1-DREADD (**c,f**) mice in the EPM test following administration of vehicle (**a–c**) or 0.3 mg kg⁻¹ CNO (**d–f**) (i.p., 30 min before the test). Heat maps represent the occupancy (blue, 0 s occupancy; red, 5 s occupancy) of 2–6 mice per treatment group. **g**, Mean anxiety level of WT, M1-KO or M1-DREADD mice treated with vehicle or CNO (calculated as the ratio of open/closed arm entries divided by the total number of entries) before the EPM test. Data represent 16–26 individual mice, and were analyzed using a two-way analysis of variance (ANOVA) with a Sidak’s multiple comparison test (* $P < 0.05$, ** $P < 0.01$, *** $P < 0.001$). **h–j**, Representative motion plots of WT (**h**), M1-KO (**i**) or M1-DREADD (**j**) mice in the open field test. **k**, Average distance traveled by WT, M1-KO or M1-DREADD mice over a 10 min period in the open field test. Inset: total distance traveled for each genotype over a 10 min period). Data are presented as means of 3–5 separate mice. **l**, Total distance traveled in an 8 min period by WT, M1-KO or M1-DREADD following administration of vehicle or 0.3 mg kg⁻¹ CNO 30 min before a Y maze test. Data are presented as mean \pm s.e.m. of 4–13 individual mice, and were analyzed using a two-way ANOVA with a Sidak’s multiple comparison test (** $P < 0.01$, *** $P < 0.001$).

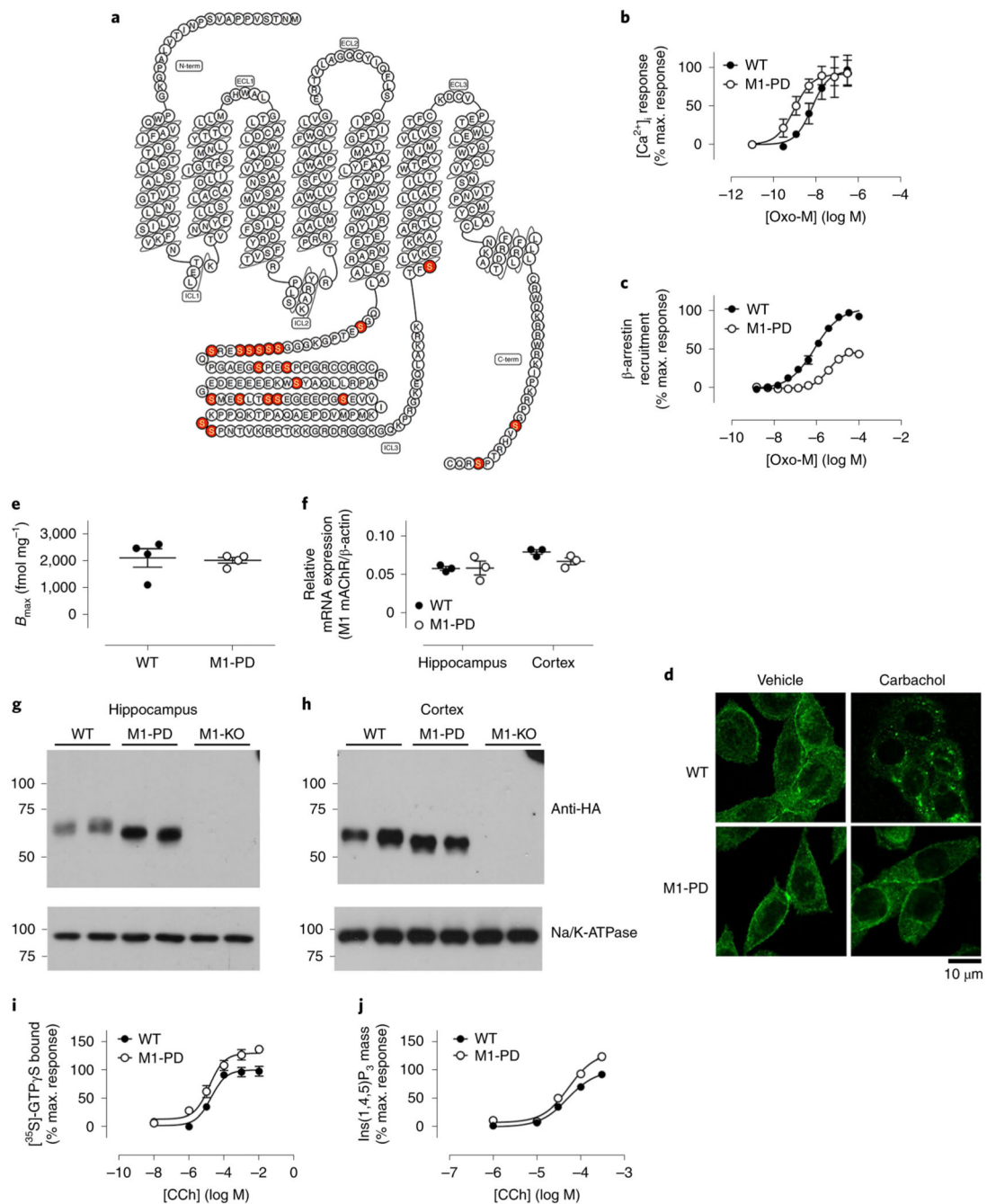


Fig. 3. Generation of the G protein-biased M1-PD knock-in mouse.

a, Snake plot of the M1 receptor identifying the mutations introduced to generate the M1-PD receptor. **b**, Stimulation of intracellular Ca^{2+} release in HEK cells transiently transfected with mouse M1 WT or M1-PD mAChRs. **c**, β -arrestin recruitment to the M1 mAChR determined using PathHunter HEK cells expressing either the M1-WT or M1-PD receptor. Shown are concentration–response curves to the full muscarinic-receptor agonist oxotremorine-M (oxo-M). Data are presented as mean \pm s.e.m. of three independent experiments and are expressed as a percentage of the maximal response to Oxo-M at the

WT M1 mAChR. **d**, Representative images showing the localization of HA-tagged M1 WT or M1-PD in CHO cells stimulated with vehicle or 100 μ M carbachol for 1 h before fixation with 4% paraformaldehyde (PFA) ($\times 63$ objective). Data shown are representative of four individual experiments. **e**, [3 H]-*N*-methyl scopolamine (NMS) binding to cortical membranes prepared from WT M1-HA or M1-PD mice ($n = 4$). Data are presented as mean \pm s.e.m. **f**, qRT-PCR showing the transcription of M1 mAChR RNA in the hippocampus or cortex of WT and M1-PD mice. Data are expressed as a ratio of β -actin RNA transcription ($n = 3$ mice). **g,h**, Solubilized membranes prepared from the hippocampus (**g**) or cortex (**h**) of WT M1-HA, M1-PD and M1-KO mice were probed in a western blot analysis for the expression of M1 mAChR using an antibody for the HA tag. Data shown are for two separate mice for each genotype; similar data were obtained on at least two further occasions (Supplementary Fig. 6). Na⁺K⁺ATPase expression was used as a loading control. **i,j**, Stimulation of [35 S]-GTP γ S G_{q/11} binding (**i**) or Ins(1,4,5)P₃ accumulation (**j**) in cortical tissue prepared from WT or M1-PD mice following stimulation with CCh. Data are expressed as mean \pm s.e.m. of three independent experiments performed in duplicate ([35 S]-GTP γ S) or triplicate (Ins(1,4,5)P₃ accumulation) and normalized to the maximal response at the WT receptor.

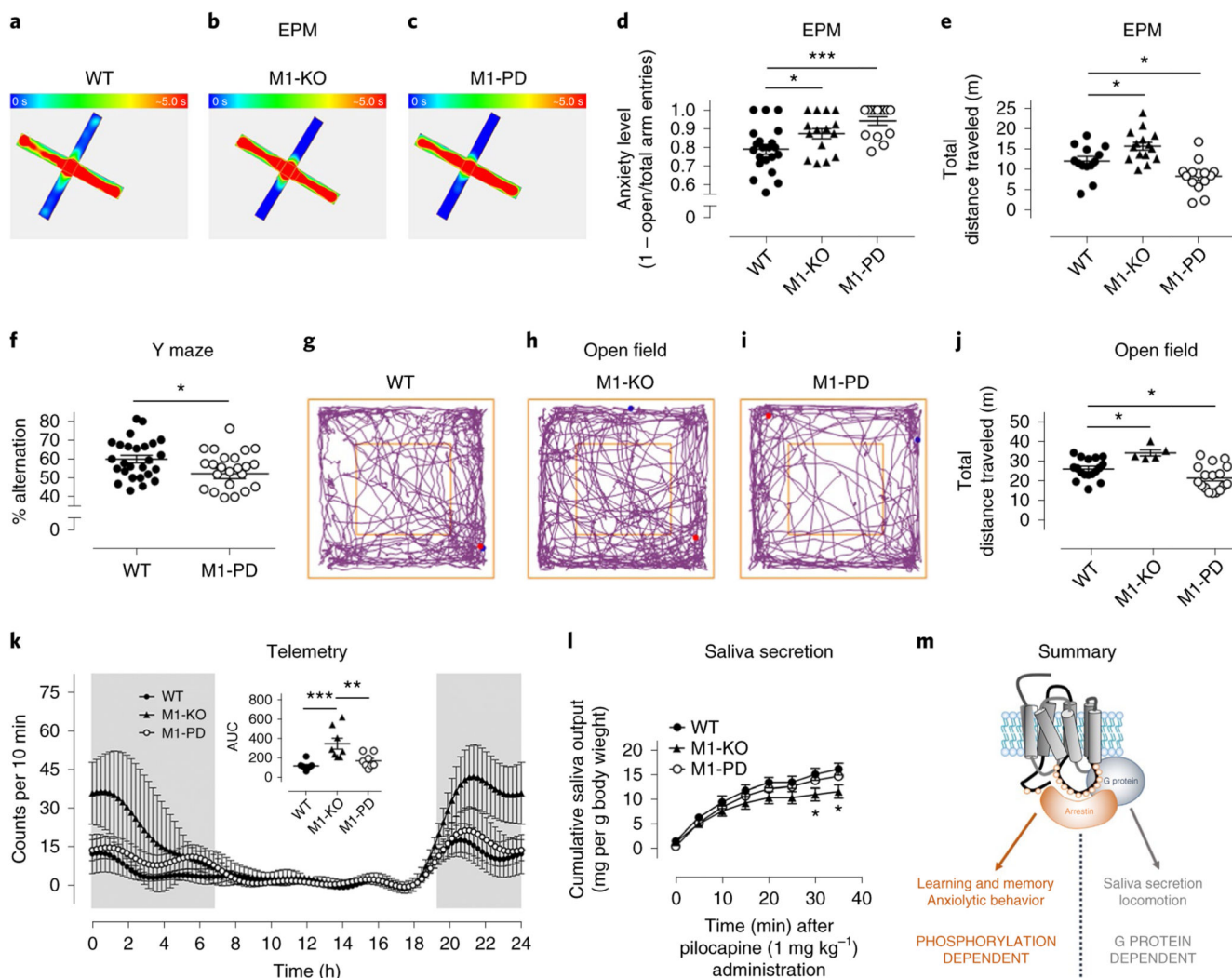


Fig. 4. Mapping of bimodal signaling to M1 mAChR physiological responses.

a–c, Heat maps showing the occupancy of WT (**a**, $n = 13$), M1-KO (**b**, $n = 4$) or M1-PD (**c**, $n = 14$) mice in the open or closed arms of the EPM (blue, 0 s occupancy; red, 5 s occupancy). **d**, Anxiety level of WT ($n = 21$), M1-KO ($n = 15$) or M1-PD ($n = 14$) mice (calculated as a ratio of open/closed arm entries divided by the total number of entries). **e**, Total distance traveled in the EPM of WT ($n = 13$), M1-KO ($n = 15$) or M1-PD ($n = 14$) mice. Data in **d** and **e** are presented as mean \pm s.e.m. and were analyzed using a one-way ANOVA with Dunnett's multiple comparisons test. $*P < 0.05$; $***P < 0.001$. **f**, WT or M1-PD mice were tested for 8 min in a Y maze spontaneous alternation paradigm to assess spatial working memory. Data are presented as mean \pm s.e.m. and were analyzed using a Student's t -test. $*P < 0.05$. **g–i**, Representative track plots of WT (**g**), M1-KO (**h**) and M1-PD (**i**) mice in the open field test. **j**, Total distance traveled in a 10 min period by WT, M1-KO and M1-PD mice during an open field test. Data are presented as mean \pm s.e.m. and were analyzed using a one-way ANOVA with Dunnett's multiple comparisons test. $*P < 0.05$. **k**, Basal locomotor activity of WT, M1-KO and M1-PD mice, assessed using in vivo telemetry recordings. Mean locomotor activity \pm s.e.m. of eight mice over a 24 h period

is shown, with total locomotor activity during this period calculated by measurement of the area under the curve (AUC). **l**, Salivary secretion in response to pilocarpine (1 mg kg^{-1}) administration was measured in WT, M1-KO and M1-PD mice. Data are presented as mean \pm s.e.m. of $n = 5-7$ mice. Data were analyzed using a one-way ANOVA with Dunnett's multiple comparisons test compared to WT mice. $*P < 0.05$. **m**, An illustration of the M1 mAChR physiological responses lying downstream of G protein-dependent signaling (saliva secretion and locomotion) versus phosphorylation-dependent signaling (anxiolytic behavior and spatial working memory).

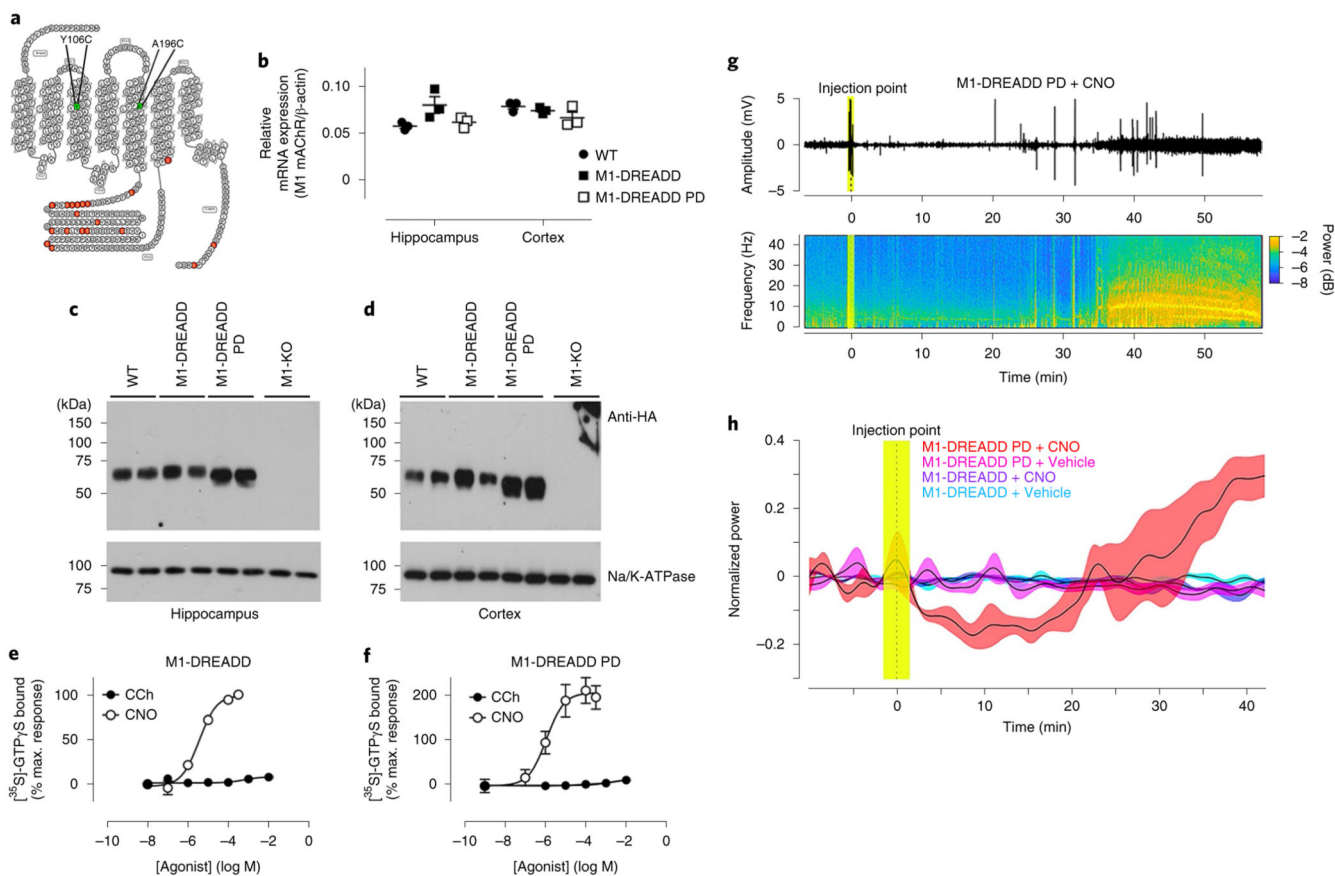


Fig. 5. M1-DREADD PD mice show epileptic-like seizures.

a, Snake plot of the M1 mACHR identifying the mutations introduced to generate the M1-DREADD PD receptor. **b**, qRT-PCR showing the transcription of M1 mACHR RNA in the hippocampus or cortex of WT, M1-DREADD or M1-DREADD PD mice. Data are expressed as a ratio of β -actin RNA transcription ($n = 3$ mice). **c, d**, Solubilized membranes prepared from the hippocampus (**c**) or cortex (**d**) of WT, M1-DREADD, M1-DREADD PD and M1-KO mice were probed in a western blot analysis for the expression of M1 mACHR using an antibody for the HA tag. Data shown are for two separate mice for each genotype. Similar data were obtained on at least two further occasions (Supplementary Fig. 2). Na⁺K⁺ATPase expression was used as a loading control. **e, f**, Stimulation of [³⁵S]-GTP γ S binding to cortical membranes prepared from M1-DREADD (**e**) or M1-DREADD PD (**f**) mice following stimulation with CCh or CNO. Data are expressed as mean \pm s.e.m. of 3–4 independent experiments performed in duplicate and normalized to the maximal response at the WT receptor. **g**, Raw cortical electroencephalogram (EEG) signals (top) and the spectrogram (bottom) in a representative M1-DREADD PD mouse following administration of CNO (0.3 mg kg⁻¹, i.p.) after 15 min of recording basal cortical activity. **h**, Normalized EEG power in M1-DREADD or M1-DREADD PD mice treated with vehicle (5% glucose) or CNO (0.3 mg kg⁻¹). Data are presented as mean \pm s.e.m. of 4–8 individual mice and were analyzed using a repeated measures ANOVA, $F(3, 3,119) = 5.53$, $P = 0.029$.

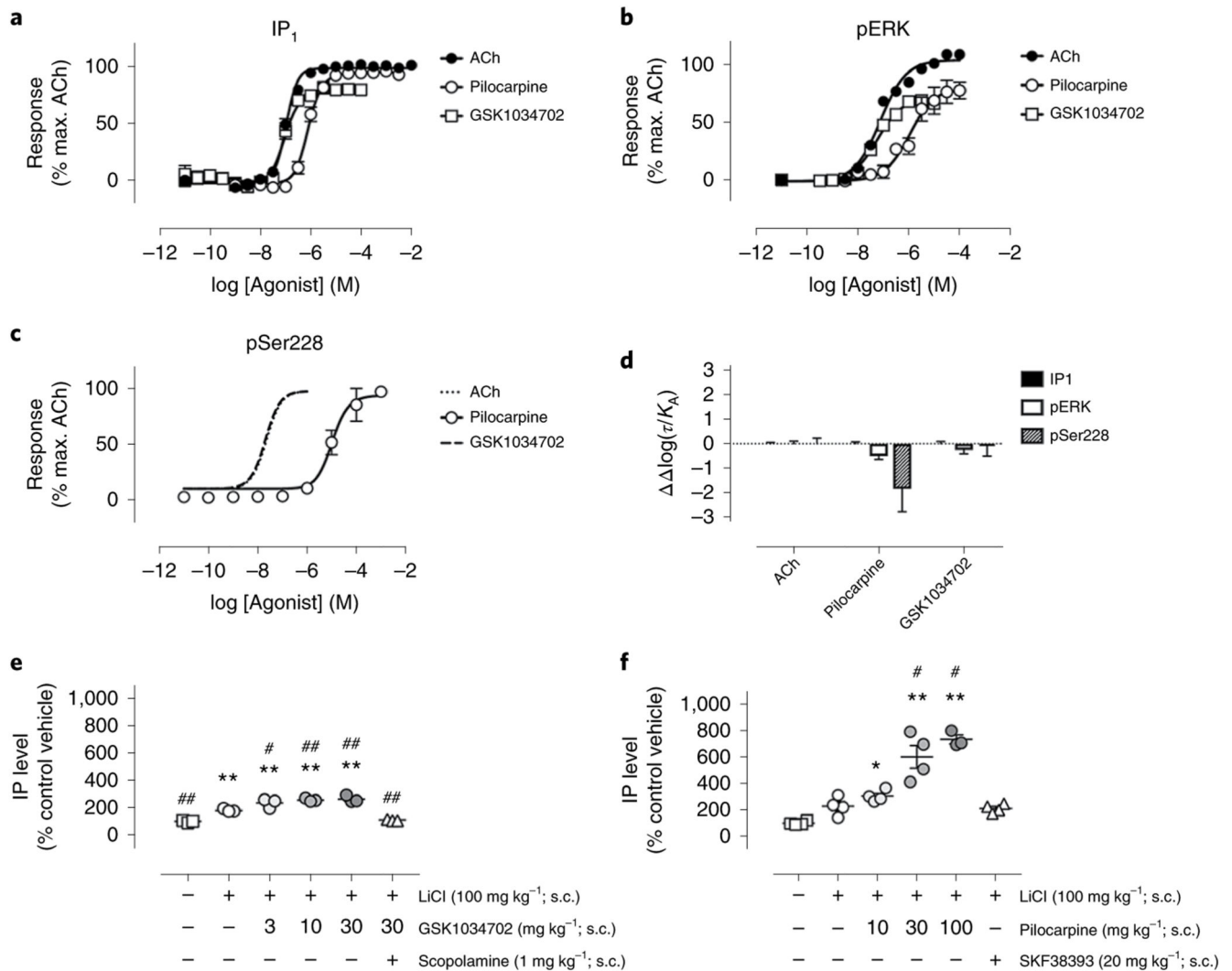


Fig. 6. Pilocarpine shows G protein bias, whereas GSK1034702 is not biased.

a–c, Inositol phosphate (IP₁) accumulation (**a**), ERK1/2 phosphorylation (pERK) (**b**) or M1 mAChR phosphorylation at serine 228 (pSer228) (**c**) stimulated by acetylcholine (ACh), pilocarpine or GSK1034702 in CHO cells stably expressing the mouse WT M1 mAChR. Dashed lines show data generated as part of a previous dataset for comparison¹⁰. **d**, Preferential signaling bias ($\Delta\Delta\log(\tau/K_A)$) stimulated by ACh, pilocarpine and GSK1034702 towards IP₁, pERK or pSer228 pathways at the WT M1 receptor. Data are presented as mean \pm s.e.m. and used ACh as the reference ligand. **e,f**, Stimulation of inositol phosphate accumulation in the frontal cortex of male Sprague–Dawley rats followed by administration of increasing concentrations of GSK1034702 (**e**) or pilocarpine (**f**). SKF38393 is a D1 dopamine receptor agonist. Data are presented as mean \pm s.e.m. of 3–4 rats and were analyzed using a two-way ANOVA with Dunnett’s multiple comparison. * $P < 0.05$, ** $P < 0.01$ versus vehicle; # $P < 0.05$, ## $P < 0.01$ versus LiCl.